Monthly Notices of the ROYAL ASTRONOMICAL SOCIETY
MNRAS **448,** 2312–2331 (2015) doi:10.1093/mnras/stv106

SN 2012ec: mass of the progenitor from PESSTO follow-up of the photospheric phase

C. Barbarino,[1,2★] M. Dall'Ora,[2] M. T. Botticella,[2] M. Della Valle,[2,3] L. Zampieri,[4] J. R. Maund,[5] M. L. Pumo,[4] A. Jerkstrand,[6] S. Benetti,[4] N. Elias-Rosa,[4] M. Fraser,[7] A. Gal-Yam,[8] M. Hamuy,[9,10] C. Inserra,[6] C. Knapic,[11] A. P. LaCluyze,[12] M. Molinaro,[11] P. Ochner,[4] A. Pastorello,[4] G. Pignata,[9,13] D. E. Reichart,[12] C. Ries,[14] A. Riffeser,[14] B. Schmidt,[15] M. Schmidt,[14] R. Smareglia,[11] S. J. Smartt,[6] K. Smith,[6] J. Sollerman,[16] M. Sullivan,[17] L. Tomasella,[4] M. Turatto,[4] S. Valenti,[18] O. Yaron[8] and D. Young[6]

Affiliations are listed at the end of the paper

Accepted 2015 January 14. Received 2015 January 14; in original form 2014 October 28

ABSTRACT

We present the results of a photometric and spectroscopic monitoring campaign of SN 2012ec, which exploded in the spiral galaxy NGC 1084, during the photospheric phase. The photometric light curve exhibits a plateau with luminosity $L = 0.9 \times 10^{42}$ erg s^{-1} and duration ∼90 d, which is somewhat shorter than standard Type II-P supernovae (SNe). We estimate the nickel mass $M(^{56}\mathrm{Ni}) = 0.040 \pm 0.015$ M$_\odot$ from the luminosity at the beginning of the radioactive tail of the light curve. The explosion parameters of SN 2012ec were estimated from the comparison of the bolometric light curve and the observed temperature and velocity evolution of the ejecta with predictions from hydrodynamical models. We derived an envelope mass of 12.6 M$_\odot$, an initial progenitor radius of 1.6×10^{13} cm and an explosion energy of 1.2 foe. These estimates agree with an independent study of the progenitor star identified in pre-explosion images, for which an initial mass of $M = 14-22$ M$_\odot$ was determined. We have applied the same analysis to two other Type II-P SNe (SNe 2012aw and 2012A), and carried out a comparison with the properties of SN 2012ec derived in this paper. We find a reasonable agreement between the masses of the progenitors obtained from pre-explosion images and masses derived from hydrodynamical models. We estimate the distance to SN 2012ec with the standardized candle method (SCM) and compare it with other estimates based on other primary and secondary indicators. SNe 2012A, 2012aw and 2012ec all follow the standard relations for the SCM for the use of Type II-P SNe as distance indicators.

Key words: supernovae: general – supernovae: individual: SN 2012ec – supernovae: individual: SN 2012aw – supernovae: individual: SN 2012A – supernovae: individual: NGC 1084.

1 INTRODUCTION

Core-collapse supernovae (CC-SNe) originate from the gravitational collapse of the iron cores formed by massive stars ($M \geq 8$ M$_\odot$) that cannot be supported by further exothermal thermonuclear reactions (Iben & Renzini 1983; Woosley, Heger & Weaver 2002). An important sub-class of CC-SNe is represented by Type II-plateau events (SNe II-P) characterized by the presence of hydrogen in their spectra (Filippenko 1997) and a luminosity 'plateau' that lasts for ∼80–100 d, after the blue-band maximum of the light curve (Barbon, Ciatti & Rosino 1979). The plateau is powered by the recombination of hydrogen in the SN ejecta. When the recombination ends, the light curve drops sharply by several magnitudes in ∼30 d (e.g. Kasen & Woosley 2009; Olivares et al. 2010). This transition phase is followed by a linear 'radioactive tail', where the light curve is powered by the radioactive decay of ^{56}Co–^{56}Fe. In this phase, the SN luminosity depends on the amount of ^{56}Ni synthesized in the explosion (e.g. Weaver & Woosley 1980).

Both theoretical (e.g. Grassberg, Imshennik & Nadyozhin 1971; Litvinova & Nadezhin 1983; Utrobin & Chugai 2008; Pumo & Zampieri 2011; Bersten et al. 2012) and empirical (e.g. Smartt, Eldridge & Crockett 2009) investigations show that Type II-P SNe are generally associated with red supergiants (RSGs). A minor

★ E-mail: cristina.barbarino@gmail.com

fraction of them (less than 3–5 per cent; e.g. Smartt et al. 2009; Kleiser et al. 2011; Pastorello et al. 2012) results from the explosion of a blue supergiant, similar to SN 1987A (Gilmozzi et al. 1987; Kirshner et al. 1987). Theoretical models predict that Type II-P SNe are the final fate of progenitors between 8 and 30 $M_{\odot}$ (e.g. Heger et al. 2003; Walmswell & Eldridge 2012). Most progenitors identified in high-resolution archival images were found to be RSGs of initial masses between ∼8 and ∼17 $M_{\odot}$. The apparent lack of high-mass progenitors has been dubbed as the 'RSG problem' (Smartt et al. 2009, and references therein). The existence of this discrepancy has been further confirmed by studies of the massive star population in Local Group galaxies, for which RSGs have been found to have masses up to 25 $M_{\odot}$ (Massey, Waterhouse & DeGioia-eastwood 2000; Massey, DeGioia-eastwood & Waterhouse 2001).

The reason for this lack of detection of massive RSG progenitors is still debated. A possible solution of the RSG problem was presented by Walmswell & Eldridge (2012). They speculate that an underestimation of the luminosity of the RSG SN progenitors (and therefore of their masses) might occur if we neglect the presence of an additional extinction due to dust production in the RSG winds. They estimated a new upper limit for the mass range of $21^{+2}_{-1}\,M_{\odot}$, which is, within the errors, marginally consistent with the range derived by Smartt (2009). Kochanek, Khan & Dai (2012) pointed out that the use of standard interstellar extinction laws may overestimate the effects of the reddening.

A different approach to estimate the mass of Type II-P SN progenitors is based on the use of hydrodynamic modelling of the SN evolution. This allows us to determine the ejecta mass, explosion energy, pre-SN radius and Ni mass by performing a simultaneous comparison between the observed and simulated light curves, the evolution of line velocities and the continuum temperature (Litvinova & Nadezhin 1983, 1985; Zampieri 2005, 2007). The pre-explosion mass is calculated from the ejecta mass assuming the mass of a neutron star remnant (1.4 $M_{\odot}$) and mass-loss through stellar winds. The hydrodynamic modelling of several well-observed Type II-P SNe (SNe 1997D, Zampieri, Shapiro & Colpi 1998; 1999em, Elmhamdi, Danziger, Chugai 2003a; 2003Z, Utrobin, Chugai & Pastorello 2007 and Spiro, Pastorello & Pumo 2014; 2004et, Maguire et al. 2010; 2005cs, Pastorello et al. 2009a; 2009kf, Botticella et al. 2010) determined higher masses for the progenitors than those derived from the analysis of pre-explosion images. This discrepancy either points to systematic errors in the analysis of pre-explosion images or in the assumptions in the physics of the hydrodynamical modelling (Utrobin 1993, 2007; Blinnikov et al. 2000; Chugai & Utrobin 2000; Zampieri et al. 2003; Pastorello et al. 2004, 2009b; Utrobin et al. 2007; Utrobin & Chugai 2008, 2009).

Another method to estimate the mass of the progenitor is the modelling of nebular phase spectroscopic observations (Jerkstrand et al. 2012, 2014b), which provide good agreement with estimates obtained by the analysis of pre-explosion images.

The astrophysical interest in Type II-P SNe is twofold: (1) observations show that Type II-P SNe are the most common explosions in the nearby Universe (e.g. Cappellaro, Evans & Turatto 1999; Li et al. 2011); and (2) starting from the pioneering suggestion by Kirshner & Kwan (1974), Type II-P SNe have been proposed as robust distance indicators. Two different approaches are used to derive distance measurements of SNe II-P. The theoretical approach is based on spectral modelling like the EPM method (e.g. Eastman, Schmidt & Kirshner 1996) or the spectral expanding atmosphere method (e.g. Baron et al. 2004). Empirical approaches exploit the observed correlation between the luminosity of a Type II-P SN and its expansion velocity (e.g. the standardized candle method – SCM; Hamuy & Pinto 2002) or the steepness of the light curve after the plateau phase (Elmhamdi, Chugai & Danziger 2003b). The Hamuy & Pinto (2002) method, refined for example by Nugent et al. (2006), Poznanski et al. (2009) and Olivares et al. (2010), has an intrinsic accuracy of ∼10–12 per cent (Hamuy & Pinto 2002); slightly larger than the accuracy obtained for Type Ia SNe (e.g. Tammann & Reindl 2013). Type II-P SNe can, importantly, be observed out to cosmological distances (e.g. Nugent et al. 2006), with the advantage being that they arise from a homogenous progenitor population. The Hamuy & Pinto (2002) method can, therefore, be used as an independent health check of the SN Ia-based distance scale.

The main goal of this paper is to present the results of our photometric and spectroscopic monitoring campaign of SN 2012ec, which exploded in NGC 1084. The early data were collected via the Large Programme 'Supernova Variety and Nucleosynthesis Yelds' (PI: S. Benetti). A substantial fraction of the data has been collected via the ESO Public Survey PESSTO [1] ('Public ESO Spectroscopic Survey of Transient Objects', PI: S. J. Smartt). The observations of SN 2012ec were analysed in conjunction with the hydrodynamical codes described in Pumo, Zampieri & Turatto (2010) and Pumo & Zampieri (2011), and information on the progenitor obtained from high-resolution pre-explosion images. The same analysis has already performed for two other Type II-P SNe: SN 2012A (Tomasella et al. 2013; Roy et al. 2014) and SN 2012aw (Fraser et al. 2012; Bayless et al. 2013; Bose et al. 2013; Dall'Ora et al. 2014). This allows us to carry out a homogeneous comparative study of these three SNe, and to identify possible systematic discrepancies in the estimates of the masses of the progenitors derived from different techniques.

The paper is organized as follows: in Section 2, we present the discovery and the detection of the progenitor of SN 2012ec; in Section 3, we discuss the properties of the host galaxy, the distance and the extinction; in Section 4, we present the optical and near-infrared (NIR) photometric evolution of SN 2012ec, and compare its colour evolution and bolometric light curve with those of other Type II-P SNe. In Section 5, we present the optical and NIR spectroscopic observations. In Section 6, we discuss the results of the modelling of the data, and in Section 7 we present a detailed comparison of SN 2012ec with the Type II-P SNe 2012A and 2012aw. In Section 8, we consider these three SNe in the context of the SCM, and in Section 9 we discuss our results.

2 DISCOVERY AND PROGENITOR DETECTION

SN 2012ec was discovered by Monard (2012) in the almost face-on ($i = 57^{\circ}$; Moiseev 2000) spiral galaxy NGC 1084 on 2012 August 11.039 UT (MJD=56150.04). Childress et al. (2012) classified SN 2012ec as a very young Type II-P SN, probably a few days post-explosion. In Fig. 1, we show this early spectrum of SN 2012ec (collected on 2012 August 13 with Wide-Field Spectrograph – WiFeS; MJD =56152.2), compared with SN 2006bp (Quimby et al. 2007) at five different epochs. The spectrum of SN 2012ec is very similar to those of SN 2006bp (Quimby et al. 2007) obtained at 8 and 10 d after the explosion, implying that the SN was observed at ∼+ 9 d post-explosion and giving an explosion epoch of ∼7 d before the discovery. We explicitly note that our estimate is slightly

[1] www.pessto.org

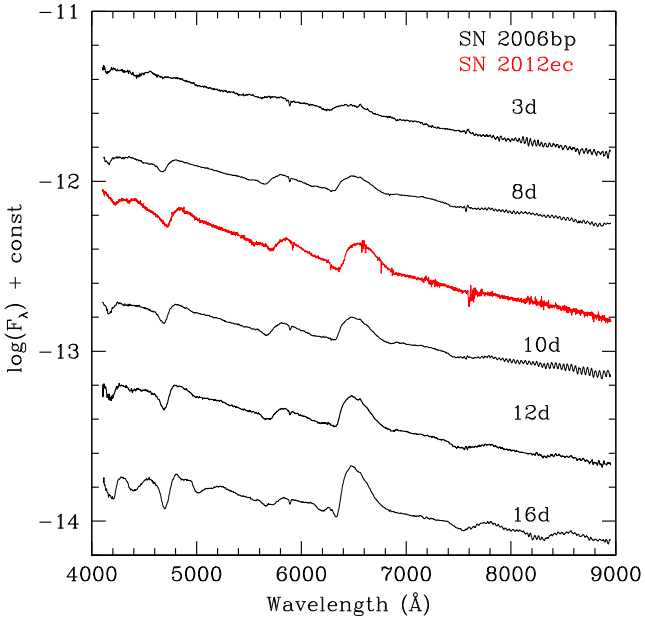

Figure 1. Comparison between a very early spectrum of SN 2012ec and five spectra of SN 2006bp, from day 3 to 16.

different from the one given by Maund et al. (2013), who estimated the explosion date at < 6 d before the discovery by comparison with spectra of SN 1999em. The explosion epoch of SN 2006bp is much more tightly constrained than that of SN 1999em, because it is based on the detection of shock breakout (Nakano 2006; Quimby et al. 2007). The estimates obtained by using either SN 2006bp or SN 1999em, as reference, are in agreement within the errors. We adopt, therefore, a conservative constraint on the explosion date of 7 ± 2 d prior to discovery and define the zero phase as our estimated explosion epoch of MJD = 56143.0.

Maund et al. (2013) identified a progenitor candidate in pre-explosion *Hubble Space Telescope* images. Photometry of the progenitor candidate was compared with synthetic photometry of MARCS spectral energy distributions (SED; Gustafsson et al. 2008), which suggested that the progenitor of SN 2012ec was an RSG with an initial mass in the range 14–22 $M_\odot$.

3 HOST GALAXY, DISTANCE AND EXTINCTION

The SN is located 0.7″E and 15.9″N of the nucleus of the host galaxy NGC 1084 (see Fig. 2). Details of NGC 1084 are presented in Table 1. NGC 1084 previously hosted four known SNe: the Type II-P SN 2009H (Li, Cenko & Filippenko 2009), the Type II SNe 1998dl (King et al. 1998) and 1996an (Nakano et al. 1996) and the Type Ia SN 1963P (Kowal 1968).

The distances available in the literature for NGC 1084 are principally based on the Tully–Fisher relation, and we adopt the value $\mu = 31.19 \pm 0.13$ mag, available in the Extragalactic Distance Database[2] (Tully et al. 2009).

The Galactic reddening towards SN 2012ec was estimated from the Schlafly & Finkbeiner (2011) dust maps to be $E(B-V) = 0.024$ mag.[3] The internal reddening in NGC 1084 was derived

[2] Extragalactic Distance Database: http://edd.ifa.hawaii.edu/

[3] We checked the consistency with the Schlegel, Finkbeiner & Davis (1998) calibration, and they agree within a few thousandths of magnitude.

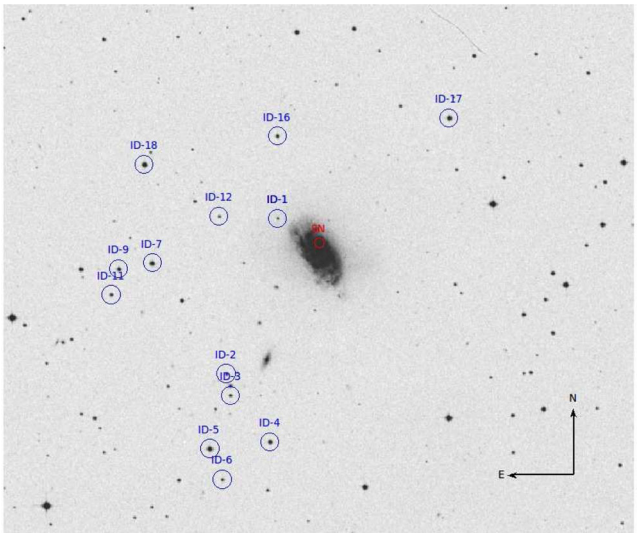

Figure 2. An image of SN 2012ec and the host galaxy NGC 1084, acquired with the Liverpool Telescope and the IO:O camera. The field of view is 14.5×14.5 arcmin^2. Reference stars are circled and labelled (see Tables 3 and 4).

Table 1. Properties of NGC 1084.

α (2000)	$2^h43^m32^s.091$
δ (2000)	$-07°47'16''.76$
Morphological type	SA(s)d
z	$0.004\,693 \pm 0.000\,013$
μ	31.19 ± 0.13 mag
$v_{\rm Hel}$	1407 ± 4 km s^{-1}
$E(B-V)_{\rm Galactic}$	0.024 mag
$E(B-V)_{\rm host}$	0.12 mag

using the measured equivalent widths (EW) of Na ID (5889, 5895 Å), observed in a low-resolution spectrum at +19 d. The measured value was EW(Na ID) $= 0.8 \pm 0.3$ Å from which we obtained $E(B-V) = 0.12^{+0.15}_{-0.12}$ mag using the Poznanski, Prochaska & Bloom (2012) calibration and $E(B-V) = 0.11$ mag using the Turatto, Benetti & Cappellaro (2003) calibration. These two values are in good agreement and we adopt $E(B-V) = 0.12^{+0.15}_{-0.12}$ mag for the host galaxy reddening.

Assuming a Cardelli, Clayton & Mathis (1989) reddening law ($R_V = 3.1$), we estimate the total Galactic and host V-band extinction towards SN 2012ec to be $A_V = 0.45$ mag.

4 PHOTOMETRIC EVOLUTION

4.1 Data sample and reduction

A photometric and spectroscopic monitoring campaign for SN 2012ec, at optical and NIR wavelengths, was conducted over a period 153 d, covering 77 epochs from 11 to 164 d post-explosion, using multiple observing facilities. Additional data collected in the nebular phase will be published in a companion paper (Jerkstrand et al. 2014a).

BVRI Johnson–Cousins data were collected with: the 2.0m Liverpool Telescope (LT, Canary Islands, Spain) equipped with the IO:O camera (*BV*, 21 epochs); the 3.58m ESO New Technology Telescope (NTT, La Silla, Chile) equipped with the EFOSC2 (ESO Faint Object Spectrograph and Camera) camera (*BVRI*, 9 epochs); the 1.82m Copernico telescope (Asiago, Italy) equipped

Table 2. Summary of the characteristics of the instruments used during for photometric monitoring.

Telescope	Camera	Pixel scale (arcsec pixel^{-1})	Field of view (arcmin^2)	Filters[a]	# of epochs
NTT (3.58m)	EFOSC2	0.24	4 × 4	*B*, *V*, *R*; *u*, *g*, *r*, *i*	12
NTT (3.58m)	SOFI	0.28	5 × 5	*J*, *H*, K_s	8
LT (2.0m)	IO:O	0.15	10 × 10	*B*, *V*; *u*, *r*, *i*, *z*	21
PROMPT (0.41m)	APU9	0.59	11 × 11	*B*, *V*, *R*, *I*; *g*, *r*, *i*, *z*	21
CAO (1.82m)	AFOSC	0.46	8 × 8	*B*, *V*, *R*; *i*	3
SAO (0.97m)	SBIG	0.86	57 × 38	*R*	1
WOT (0.4m)	SBIG ST-10 XME	0.44	16 × 10	*g*, *r*, *i*	7
TRAPPIST (0.60m)	TRAPPISTCAM	0.65	27 × 27	*B*, *V*, *R*	4

NTT = New Technology Telescope with the optical camera EFOSC2 and with the NIR camera SOFI; LT = the Liverpool Telescope with the optical CCD camera IO:O; PROMPT = Panchromatic Robotic Optical Monitoring and Polarimetry Telescopes; CAO = the Copernico telescope at Asiago Observatory with AFOSC; SAO = the Schmidt telescope at the Asiago Observatory; WOT = the 40 cm telescope at the Wendelstein Observatory; TRAPPIST = TRAnsit Planets and PlanetesImals Small Telescope.
[a]The NTT and CAO *i* filter is Gunn.

with the AFOSC – Asiago Faint Object Spectrograph and Camera – (*BVRI*; 3 epochs); the 0.6m ESO TRAnsiting Planets and PlanetesImals Small Telescope (TRAPPIST, La Silla, Chile), equipped with TRAPPISTCAM (*BVR*, 4 epochs); and the array of 0.41m Panchromatic Robotic Optical Monitoring and Polarimetry Telescopes (PROMPT, Cerro Tololo, Chile), equipped with Apogee U47p cameras, which employ the E2V CCDs (*BVRI*, 21 epochs).

ugriz images were collected with: the LT equipped with the IO:O camera (*uriz* 21 epochs); the ESO NTT telescope equipped with EFOSC2 (*ugriz*, 3 epochs); the PROMPT telescopes (*griz*, 19 epochs); and the 0.4m telescope at the Wendelstein Observatory (Mount Wendelstein, Germany), equipped with a ST-10 CCD camera (*gri*, 7 epochs).

JHK_s observations were acquired with the ESO NTT telescope, equipped with the SOFI (Son Of ISAAC) camera (8 epochs).

A summary of the characteristics of the instruments and telescopes used for photometric follow-up are presented in Table 2.

Data were pre-reduced using the respective instrument pipelines, where available, or following the standard procedures (bias, overscan and flat-field corrections, trimming) in the IRAF[4] environment. In particular, NIR images were pre-reduced by means of an IRAF-based custom pipeline based on the XDIMSUM IRAF package (Coppola et al. 2011), which conducts the background subtraction using a two-step technique based on a preliminary guess of the sky background and with a careful masking of unwanted sources in the sky images.

Johnson–Cousins *BVRI* calibrated magnitudes of 18 reference stars were obtained by averaging their photometry obtained on 12 photometric nights, in conjunction with observations of Landolt (1992) standard star fields. *ugriz* calibrated photometry for 17 reference stars were obtained on 11 photometric nights with the LT and the NTT telescopes, in conjunction with observations of Smith, Tucker & Kent (2002) $u'g'r'i'z'$ standard star fields. Finally, calibrated NIR 2MASS *JHK* photometry was obtained for five reference stars, for which 2MASS (Skrutskie et al. 2006) photometry was available. We did not correct NIR magnitudes for colour terms, since they are generally very small in the NIR bands (e.g. Carpenter 2001). Our adopted reference stars showed no clear signs of variability.

The host galaxy and the SN position are shown in Fig. 2, along with the local sequence stars adopted for the photometric calibration. The calibrated photometry for the local sequence stars is reported in Tables 3 and 4. In the following, the Johnson–Cousins *BVRI* and NIR photometry are reported in Vega magnitudes, while the *ugriz* photometry is reported in the AB magnitude system.

Photometric measurements were carried out with the `QUBA` pipeline (Valenti et al. 2011), which performs DAOPHOT-based (Stetson 1987) point-spread-function fitting photometry on the SN and on the selected reference stars. Since SN 2012ec is embedded in a spiral arm of the host galaxy, the background was estimated with a polynomial model. We performed empirical tests for the best background subtraction, and in most cases we found that a fourth-order polynomial model of the background gave satisfactory results, due to the high S/N ratio of the SN in these images. Only at the last few epochs was the S/N ratio of the SN too low to prohibit satisfactory removal of the local background. We note, however, that even using the subtraction of a template image would probably not yield a significant improvement, as in these cases the flux of the SN was only few tens of counts above the local background. Photometric uncertainties were automatically estimated by the pipeline using artificial star experiments.

The photometric measurements of the SN in the *BVRI*, $u'g'r'i'z'$ and in the *JHK* filter systems are reported in Table 5.

4.2 Data analysis

The photometric evolution of SN 2012ec in the *BVRI*, *JHK* and in the $u'g'r'i'z'$ filter systems is shown in Fig. 3.

SN 2012ec was already on the plateau in the *V*, *R*, *I*, r', i' and z' bands by +13 d. The average absolute magnitude, in the different bands, during the plateau phase was $M_V = -16.54$ mag, $M_R = -16.75$ mag, $M_I = -16.96$ mag, $M_{r'} = -16.80$ mag, $M_{i'} = -16.93$ mag and $M_{z'} = -17.08$ mag. Using the definition for the plateau duration proposed by Olivares et al. (2010), where the end of the plateau occurs at the knee of the light curve, we found that the plateau of SN 2012ec lasted almost 90 d in *R*, *I*, r', i', z' and almost 80 d in *V*. This is shorter than the usual duration of the plateau of standard Type II-P SNe (e.g. SN 2004et, 100 d, Maguire et al. 2010; SN 2012aw, 100 d, Dall'Ora et al. 2014; see also Arcavi et al. 2012). SN 2012ec began to fall from the plateau at ∼+ 90 d,

[4] IRAF is distributed by the National Optical Astronomical Observatory, which is operated by the Association of Universities for Research in Astronomy, Inc., under cooperative agreement with the National Science Foundation.

Table 3. Positions and photometry of the local sequence reference stars in the *BVRI* and in the $u'g'r'i'z'$ systems.

# id	$\alpha_{J2000.0}$ (deg)	$\delta_{J2000.0}$ (deg)	B (mag)	V (mag)	R (mag)	I (mag)	u' (mag)	g' (mag)	r' (mag)	i' (mag)	z' (mag)
1	41.521 6674	−7.559 7940	17.98 (0.02)	16.88 (0.02)	16.19 (0.02)	15.53 (0.03)	19.85 (0.02)	17.48 (0.04)	16.41 (0.01)	16.01 (0.02)	15.86 (0.01)
2	41.549 6917	−7.641 6869	16.84 (0.02)	15.97 (0.02)	15.46 (0.02)	14.93 (0.03)	18.27 (0.02)	16.43 (0.02)	15.67 (0.02)	15.38 (0.01)	15.32 (0.02)
3	41.547 4764	−7.653 0580	17.14 (0.02)	16.28 (0.02)	15.81 (0.02)	15.32 (0.02)	18.45 (0.06)	16.71 (0.03)	16.04 (0.02)	15.78 (0.01)	15.72 (0.01)
4	41.526 5649	−7.677 8087	15.58 (0.02)	14.95 (0.02)	14.66 (0.02)		16.48 (0.03)	15.25 (0.02)	14.80 (0.02)	14.64 (0.02)	14.65 (0.01)
5	41.558 9242	−7.681 1761	14.27 (0.02)	13.52 (0.02)	13.23 (0.02)		15.18 (0.02)	13.91 (0.02)	13.31 (0.02)	13.05 (0.02)	12.94 (0.01)
6	41.552 2025	−7.697 3300	17.01 (0.02)	16.00 (0.02)	15.43 (0.02)		18.82 (0.05)	16.55 (0.03)	15.62 (0.02)	15.30 (0.02)	15.18 (0.01)
7	41.588 6692	−7.582 9251	14.62 (0.01)	14.07 (0.01)	13.84 (0.02)		15.36 (0.03)	14.49 (0.02)	13.98 (0.01)	13.86 (0.02)	13.87 (0.01)
9	41.606 5545	−7.585 8940	15.16 (0.01)	14.42 (0.01)	14.08 (0.02)		16.11 (0.02)	15.03 (0.03)	14.25 (0.02)	14.04 (0.02)	14.01 (0.01)
11	41.610 8998	−7.599 6059	16.99 (0.01)	16.36 (0.01)	16.04 (0.02)		17.64 (0.02)	16.66 (0.03)	16.21 (0.01)	15.99 (0.02)	15.97 (0.02)
12	41.552 8922	−7.558 5795	18.32 (0.02)	16.83 (0.02)	15.93 (0.02)	14.73 (0.02)	20.12 (0.05)	17.65 (0.01)	16.19 (0.01)	15.24 (0.02)	14.90 (0.02)
16	41.521 5760	−7.516 7457	16.06 (0.01)	15.26 (0.01)	14.90 (0.02)	14.48 (0.01)	17.25 (0.04)	15.64 (0.03)	15.10 (0.02)	14.93 (0.02)	14.86 (0.01)
17	41.430 0180	−7.507 6398	14.74 (0.01)	14.08 (0.01)	13.81 (0.02)		14.92 (0.02)	14.43 (0.02)	14.18 (0.02)	13.92 (0.01)	13.95 (0.01)
18	41.592 5440	−7.531 0037	16.06 (0.01)	13.76 (0.01)	14.90 (0.02)						

Table 4. Positions and photometry of the local sequence reference stars in the 2MASS *JHK* system.

Star ID	$\alpha_{J2000.0}$ (deg)	$\delta_{J2000.0}$ (deg)	J (mag)	H (mag)	K (mag)
1	41.521 6674	−7.559 7940	14.82 (0.04)	14.08 (0.05)	13.94 (0.05)
2	41.549 6917	−7.641 6869	14.32 (0.03)	13.87 (0.04)	13.73 (0.05)
3	41.547 4764	−7.653 0580	14.71 (0.04)	14.35 (0.05)	14.14 (0.06)
12	41.552 8922	−7.558 5795	13.63 (0.03)	13.01 (0.03)	12.81 (0.03)

while the photospheric phase from the observed spectroscopic evolution (see Section 5.2) lasted until ∼160 d. The decline in the light curve of SN 2012ec, from the plateau to the radioactive decay tail, lasted ∼30 d, decreasing 1.5 mag in r', i', V bands, 1 mag in the I bands and 1.3 mag in the z' band. A list of the main characteristics of the light curve, for each filter, is reported in Table 6.

The NIR light curve exhibits a plateau of duration ∼90–100 d, which subsequently drops over a period of 40 d by 1.3 mag in the J band, 1.1 mag in the H band and 1.2 mag in the K band. This behaviour is similar to that observed for other Type II-P SNe (see for example, SN 2012A, Tomasella et al. 2013; SN 2012aw, Dall'Ora et al. 2014).

The evolution of the $B-V$, $V-R$ and $V-K$ colours of SN 2012ec are shown in Fig. 4. The $B-V$ colour becomes progressively redder over the first 50 d, rising from $B-V\sim 0$ to ∼1 mag, before reaching a constant value by ∼160 d. The $V-K$ colour starts from 0.7 mag and increases slowly to ∼1 mag at ∼100 d, before increasing further from ∼1 to ∼1.9 mag in the period 100–130 d. The colour evolution of SN 2012ec is similar to those of other Type II-P SNe (e.g. SN 2004et, Maguire et al. 2010; SN 1999em, Elmhamdi et al. 2003a; SN 2009bw, Inserra et al. 2012). The trends in the colour evolution are similar to those observed by Faran et al. (2014, see their fig. 10) for a sample of 23 Type II-P SNe.

4.3 Bolometric light curve and ^{56}Ni mass

A pseudo-bolometric light curve was calculated by integrating over the optical and NIR photometry. The $u'Bg'Vr'Ri'Iz'JHK$ apparent magnitudes have been converted into monochromatic fluxes at the effective wavelength for each filter, and then corrected for extinction (Section 3). The resulting SED was integrated over the entire wavelength range, assuming zero flux at the limits. The estimation of the flux was performed at only those phases for which V-band observations were available. If photometry for other bands was not available, the magnitudes were estimated at these phases by interpolating the values from photometry acquired on adjacent nights. The final integrated fluxes were converted to luminosity through application of the adopted distance modulus. The pseudo-bolometric light curve of SN 2012ec is shown in Fig. 5. The luminosity at the first epoch for which the calculation could be conducted (14 d) was $L = 1.4 \times 10^{42}\,\mathrm{erg\,s^{-1}}$; this can be considered a lower limit for the bolometric luminosity. The SN luminosity reaches the plateau by day 20 ($L = 0.9 \times 10^{42}\,\mathrm{erg\,s^{-1}}$), which then begins to significantly decrease at ∼90 d to the tail at day 130, with a luminosity of $L = 0.1 \times 10^{42}\,\mathrm{erg\,s^{-1}}$.

A comparison of the pseudo-bolometric light curve of SN 2012ec with other Type II-P SNe demonstrates a similar behaviour (e.g. SN 2012A, Tomasella et al. 2013; SN 2012aw, Dall'Ora et al. 2014; SN 2009kf, Botticella et al. 2010; and SN 2005cs, Pastorello et al. 2009a). From the pseudo-bolometric light curve of SN 2012ec, it is evident that its luminosity on the plateau is lower than observed for SNe 2012aw and SN 2009kf and that plateau duration is shorter than the more luminous SNe. SN 2012ec is more luminous than SN 2012A and SN 2005cs but has a behaviour more similar to SN 2012A. They have comparable plateau, even if the one of SN 2012A is a bit shorter. Instead SN 2005cs shows a different evolution of the light curve compared to SN 2012ec, especially the fall from the plateau that is longer for SN 2005cs.

We estimated the ^{56}Ni mass synthesized during the explosion, by comparing the luminosity of SN 2012ec with that of SN 1987A at similar late epochs. Assuming a similar γ-ray deposition fraction, the mass of ^{56}Ni was calculated using the relation of Bouchet, Danziger & Lucy (1991):

$$M(^{56}\mathrm{Ni})_{12ec} = M(^{56}\mathrm{Ni})_{87A} \times \frac{L_{12ec}}{L_{87A}}(\mathrm{M}_{\odot}). \quad (1)$$

For the ^{56}Ni mass of SN 1987A we adopted the weighted mean of the values reported by Arnett & Fu (1989) and Bouchet et al.

Table 5. Optical photometry in the Johnson–Cousins filters, in $u'g'r'i'z'$ bands and NIR photometry calibrated to the 2MASS system, with associated errors in parentheses.

Date	MJD	B (mag)	V (mag)	R (mag)	I (mag)	u' (mag)	g' (mag)	r' (mag)	i' (mag)	z' (mag)	J (mag)	H (mag)	K (mag)
20120814	56154.22	14.99 (0.02)	14.81 (0.02)			15.02 (0.04)		14.78 (0.02)	14.91 (0.02)				
20120815	51155.22	14.99 (0.04)	14.86 (0.04)			15.09 (0.02)		14.81 (0.02)	14.91 (0.02)				
20120817	56157.59	15.12 (0.06)	14.90 (0.06)	14.74 (0.06)	14.55 (0.05)								
20120818	56158.23	15.10 (0.03)	14.87 (0.03)			15.28 (0.05)		14.82 (0.01)	14.94 (0.01)				
20120819	56158.34	15.15 (0.06)	14.95 (0.05)	14.73 (0.06)	14.53 (0.03)			14.84 (0.05)	14.86				
20120820	56159.31	15.29 (0.05)	14.92 (0.04)	14.62 (0.05)	14.53 (0.05)		15.05 (0.07)	14.78 (0.03)	14.86 (0.06)				
20120821	56160.30	15.18 (0.07)	14.86 (0.06)	14.65 (0.03)	(14.61 (0.06)		15.13 (0.10)	14.81 (0.04)	14.89 (0.04)	14.92 (0.05)			
20120826	56165.28	15.47 (0.05)	14.93 (0.04)	14.64 (0.04)		16.35 (0.04)	15.25 (0.08)	14.80 (0.03)	14.87 (0.03)	14.92 (0.03)	14.24 (0.02)	14.04 (0.02)	13.91 (0.02)
20120828	56168.20	15.55 (0.02)	15.02 (0.02)			16.52(0.06)		14.85 (0.02)	14.93 (0.02)				
20120831	56171.08	15.67 (0.06)	14.98 (0.06)			16.69 (0.08)		14.81 (0.02)	14.94 (0.02)				
20120902	56173.09	15.76 (0.04)	14.99 (0.04)			16.98 (0.06)		14.85(0.02)	14.92 (0.02)				
20120905	56176.13	15.76 (0.04)	15.00 (0.05)	14.65 (0.06)	14.62 (0.06)	17.05 (0.07)		14.84 (0.03)	14.86 (0.03)	14.89 (0.03)			
20120909	56179.34	15.90 (0.06)	15.10 (0.06)	14.78 (0.04)	14.45 (0.02)		15.54 (0.02)		14.92		14.11 (0.03)	13.89 (0.03)	13.82 (0.03)
20120910	56180.92	15.95 (0.04)	15.14 (0.03)	14.76 (0.01)	14.51 (0.01)								
20120911	56181.59	16.05 (0.02)	15.15 (0.02)	14.79 (0.03)	14.53 (0.03)								
20120916	56186.20	16.06 (0.07)	15.10 (0.06)	14.75 (0.04)	14.49 (0.02)		15.51 (0.04)	14.89 (0.04)	14.87 (0.02)	14.85 (0.03)			
20120920	56190.24		15.12 (0.03)		14.42 (0.05)			14.89 (0.03)	14.85 (0.03)	14.87 (0.03)			
20120923	56194.87	16.15 (0.02)	15.10 (0.02)	14.78 (0.01)	14.45 (0.01)								
20120924	56195.23										14.08 (0.03)	13.89 (0.03)	13.75 (0.03)
20120926	56196.20	16.16 (0.06)	15.00 (0.05)	14.72 (0.03)		17.96 (0.09)	15.56 (0.03)	14.81 (0.03)	14.81 (0.03)	14.78 (0.03)			
20120929	56199.29		15.02 (0.03)	14.74 (0.03)	14.36 (0.01)			14.88 (0.02)	14.81 (0.02)	14.79 (0.02)			
20121001	56202.01	16.19 (0.05)	15.11 (0.05)			17.98 (0.11)		14.89 (0.02)	14.80 (0.03)	14.82 (0.02)			
20121002	56202.20	16.28 (0.04)	15.04 (0.04)	14.74 (0.04)	14.40 (0.02)		15.61 (0.06)	14.93 (0.05)	14.84 (0.04)	14.85 (0.04)			
20121004	56204.21	16.33 (0.04)	15.12 (0.03)	14.73 (0.03)	14.43 (0.02)	18.07 (0.14)	15.71 (0.04)	14.90 (0.03)	14.84 (0.02)	14.84 (0.02)			
20121007	56208.04	16.23 (0.08)	15.11 (0.08)			18.07 (0.18)		14.85 (0.02)	14.78 (0.02)	14.81 (0.03)			
20121010	56211.05	16.35 (0.04)	15.16 (0.04)			18.26 (0.10)	15.68 (0.03)	14.89 (0.01)	14.83 (0.01)	14.85 (0.02)			
20121012	56212.19	16.46 (0.06)	15.22 (0.07)	14.78 (0.03)	14.41 (0.02)			14.94 (0.02)	14.79 (0.03)	14.87 (0.03)			
20121016	56216.35										14.05 (0.03)	13.80 (0.03)	13.59 (0.03)
20121017	56217.15	16.50 (0.07)	15.22 (0.06)					14.95 (0.03)	14.89 (0.03)	14.77 (0.04)			
20121019	56220.42	16.63 (0.05)	15.28 (0.05)	14.77 (0.04)	14.41 (0.03)								
20121020	56221.06	16.58 (0.03)	15.36 (0.03)	14.8 (0.1)	14.43 (0.02)	18.68 (0.08)		14.96 (0.02)	14.86 (0.02)	14.92 (0.02)			
20121022	56223.52							15.00 (0.02)	14.85 (0.03)				
20121024	56226.45						15.99 (0.06)	15.01 (0.02)	14.91 (0.03)				
20121101	56232.13	16.79 (0.09)	15.47 (0.08)	14.95 (0.04)	14.59 (0.02)		16.00 (0.06)	15.15 (0.03)		15.05 (0.03)			
20121106	56237.12		15.63 (0.03)	15.04 (0.03)	14.67 (0.03)		16.2 (0.1)	15.26 (0.02)	15.15 (0.02)	15.16 (0.02)	14.35(0.06)	14.12 (0.06)	14.04 (0.04)
20121111	56242.13	17.1 (0.1)	15.85 (0.08)	15.26 (0.03)	14.85 (0.03)		16.38 (0.06)	15.39 (0.02)	15.29 (0.02)	15.26 (0.03)			
20121114	56245.20										14.58 (0.03)	14.34 (0.03)	14.28 (0.03)
20121115	56246.96	17.4 (0.1)	16.09 (0.10)					15.63 (0.02)	15.47 (0.02)	15.43 (0.02)			
20121117	56248.14		16.26 (0.04)	15.57 (0.05)	15.15 (0.04)								
20121119	56250.19	17.82 (0.09)	16.49 (0.08)	15.85 (0.05)	15.37 (0.05)		17.24 (0.05)	16.00 (0.02)	15.89 (0.02)	15.74 (0.03)			
20121122	56253.08	17.95 (0.10)	17.16 (0.10)	16.36 (0.07)	15.63 (0.05)		17.45 (0.10)	16.32 (0.03)	16.29 (0.03)	16.12 (0.12)			
20121204	56266.14										15.73 (0.06)	15.27 (0.08)	15.40 (0.06)
20121205	56266.93	18.5 (0.2)	17.3 (0.2)					16.65 (0.07)	16.51 (0.07)	16.40 (0.06)			
20121207	56268.94	18.60 (0.15)	17.40 (0.15)					16.80(0.1)	16.6 (0.1)	16.50 (0.06)			

Table 5 – *continued.*

Date	MJD	B (mag)	V (mag)	R (mag)	I (mag)	u' (mag)	g' (mag)	r' (mag)	i' (mag)	z' (mag)	J (mag)	H (mag)	K (mag)
20121209	56270.95	18.70 (0.13)	17.50 (0.13)					16.9 (0.1)	16.7 (0.1)	16.6 (0.1)			
20121216	56277.99							17.0 (0.1)	16.9 (0.1)	16.8 (0.1)			
20121220	56282.94	18.8 (0.2)	17.7 (0.2)	16.9 (0.2)							15.83 (0.03)	15.41 (0.03)	15.47 (0.03)
20121221	56283.10							17.1 (0.1)	17.1 (0.1)	16.9 (0.1)			
20121228	56290.00	19 (0.2)	17.9 (0.2)					17.2 (0.1)	17.2 (0.1)	17.0 (0.1)			
20130110	56302.81	19.15 (0.30)	18.0 (0.3)										
20130112	56305.66		18.0 (0.3)	17.15 (0.30)	16.75 (0.30)								

(1991), and for the bolometric luminosity we adopted the value of Bouchet et al. (1991, see also Suntzeff et al. 1988). For SN 2012ec we calculated $M(^{56}\mathrm{Ni})_{12ec} = 0.040 \pm 0.015\,\mathrm{M}_{\odot}$, which is an average of the estimates made at 138, 146 and 158 d (the reported uncertainty is the dispersion of the values computed at each epoch). The slope of the light curve in the last epochs of the data set is $0.01 \pm 0.02\,\mathrm{mag\,d^{-1}}$, in agreement with the ^{56}Co rate of decay. The data from the nebular phase are published in a companion paper (Jerkstrand et al. 2014a). Jerkstrand et al. (2014a) estimate the nickel mass from photometry at 187 and 202 d, finding a value of $0.03 \pm 0.01\,\mathrm{M}_{\odot}$, which is in good agreement with our estimate.

The evolution of the SED of SN 2012ec, based on optical and NIR photometry, is shown in Fig. 6. The observations covered the wavelength range 4000–23 000 Å. We evaluated the evolution of the SED and calculated blackbody continuum fits at each epoch. At 13 d, the best fit gives a blackbody temperature of 9600 ± 800 K, which decreases to 5300 ± 400 K by day 106. At early time, the fits were conducted using all available photometric observations. At later epochs, the bluest photometric observations were excluded from the fits as metal line blanketing, particularly due to Fe II and Ti II, at these wavelengths caused significant departures from the ideal blackbody assumption (Dessart & Hillier 2005). The *u*-band data was excluded from the fits for data after 20 d and, in addition, the *B* and *g* bands were excluded from fits for data after 50 d.

From the blackbody fit it was possible to evaluate the time evolution of the photospheric temperature of SN 2012ec. The temperature drops rapidly in the first 30 d from 9600 ± 800 K to 7000 ± 500 K, before decreasing slowly from 6500 ± 500 K to 5000 ± 400 K. The values of the temperature estimated from the blackbody fits to the photometric data are in good agreement with those derived from fits of the continuum in the observed spectra (within the uncertainties) from +30 d. During the first 30 d the spectroscopic temperature varies from 11 000 ± 900 K to 8000 ± 700 K, decreasing to 6200 ± 500 K at 50 d before reaching 5000 ± 500 K in the last epochs. The slightly higher temperatures estimated from the spectra are due to the limited spectroscopic wavelength range (4000–9000 Å) used for the continuum fits, compared to the wavelength range covered by the available photometric data. We compared the estimated temperatures with those of SNe 2009bw (Inserra et al. 2012) and 1999em (Elmhamdi et al. 2003a). SN 2012ec is cooler at earlier phases, compared to SN 2009bw which had an initial temperature of ∼12 000 K and SN 1999em which had a temperature of ∼14 300 K. At later phases, the temperatures of all three SNe converge to ∼5000 K.

5 SPECTROSCOPIC EVOLUTION

5.1 Data sample and reduction

As a PESSTO follow-up target, SN 2012ec was scheduled for a dense spectroscopic monitoring campaign at the ESO NTT at La Silla, Chile. 10 epochs of optical spectroscopy were acquired with EFOSC2 and 10 epochs of NIR spectroscopy were acquired with SOFI. The optical data set was supplemented with spectra from the following facilities: the 2.3 m telescope of the Siding Spring Observatory (New South Wales, Australia) equipped with WiFeS (2 epochs), the 2.5m Nordic Optical Telescope (NOT, Canary Islands, Spain) equipped with the Andalucia Faint Object Spectrograph and Camera (ALFOSC; 1 epoch), the 1.82m Copernico telescope (Asiago, Italy) equipped with AFOSC (3 epochs), the William Herschel Telescope (WHT, Canary Islands, Spain)

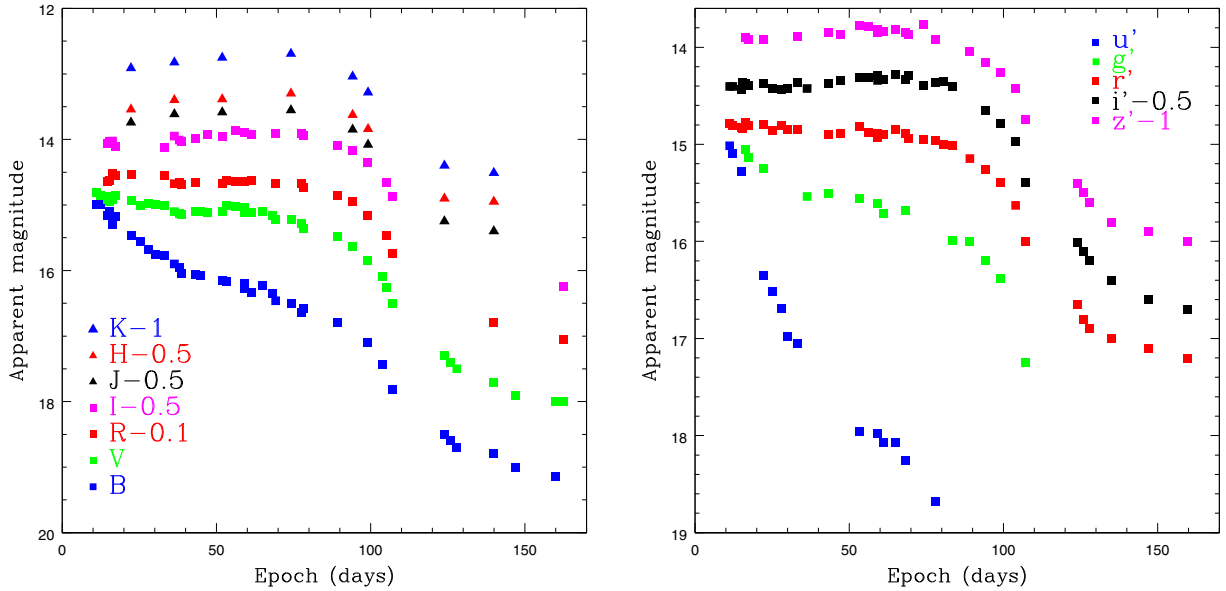

Figure 3. Left-hand panel: photometric evolution of SN2012ec in the Johnson–Cousins *BVRI* and *JHK* filters. Right-hand panel: photometric evolution of SN2012ec in the $u'g'r'i'z'$ filters. A shift has been applied for clarity.

Table 6. Epochs and apparent magnitudes of the light curve during the plateau in the $VRIr'i'z'$ bands.

	V (mag)	R (mag)	I (mag)	r' (mag)	i' (mag)	z' (mag)	J (mag)	H (mag)	K (mag)
m^a_{plat}	15.10 (0.02)	14.78 (0.01)	14.45 (0.01)	14.89 (0.03)	14.85 (0.03)	14.87 (0.03)	14.08 (0.03)	13.89 (0.03)	13.75 (0.03)
M^a_{plat}	−16.54 (0.17)	−16.75 (0.17)	−16.96 (0.17)	−16.80 (0.18)	−16.93 (0.18)	−17.08 (0.18)	−17.24 (0.18)	−17.38 (0.18)	−17.49 (0.18)

[a]Plateau phase refers to 59 d after the explosion at MJD = 56202.0.

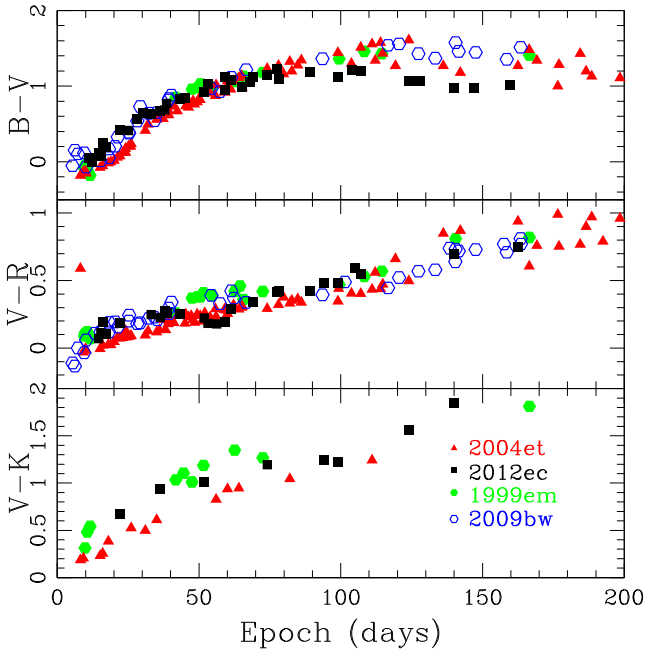

Figure 4. Colour evolution of SN 2012ec compared to other Type II-P SNe.

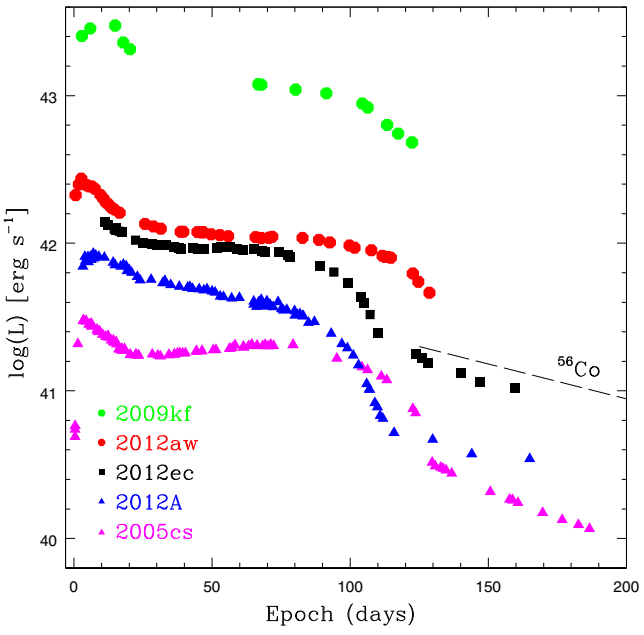

Figure 5. Pseudo-bolometric light curve of SN2012ec, along with those of other Type II-P SNe. The pseudo-bolometric light curve accounts for the *UBVRIJHK* contributions for SN 2012A, *UBgVrRiIzJHK* for SN 2012aw, *griz* for SN 2009kf and *UBVRIJHK* for SN 2005cs.

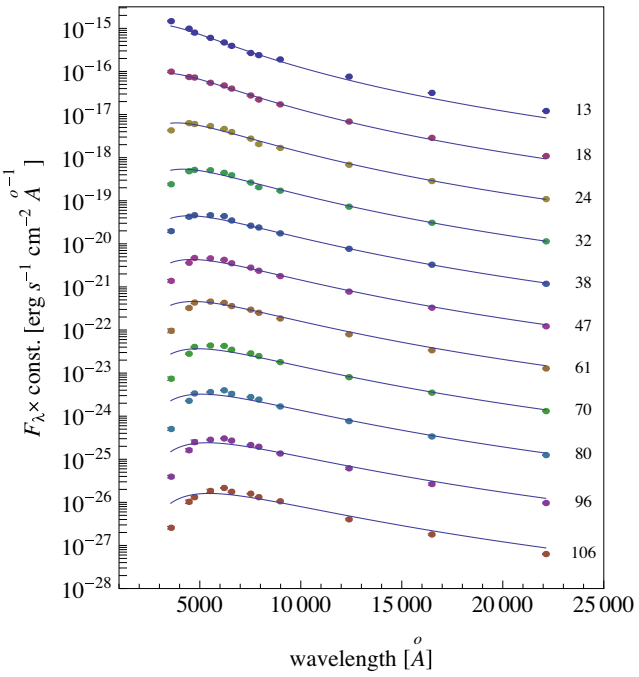

Figure 6. The temporal evolution of the SED of SN 2012ec. Circles represent the fluxes at the central wavelengths of each filter. Solid lines represent blackbody continuum fits. Fluxes are corrected for distance and extinction.

equipped with the Intermediate dispersion Spectrograph and Imaging system (ISIS; 1 epoch), the 1.22m Galileo telescope (Asiago, Italy) equipped with the Boller and Chivens spectrograph (B&C; 2 epochs). The spectroscopic observations cover 29 epochs from day 8 to 161. Details of the spectroscopic observations and the characteristics of the instruments used are listed in Table 7.

Spectra were pre-reduced (trimmed, overscan, bias and flat-field corrected) using the PESSTO pipeline (Smartt et al. 2014), based on the standard IRAF tasks.[5] The wavelength calibration was performed using comparison spectra of arc lamps acquired with the same instrumental configuration as the SN observations. The science observations were flux calibrated with respect to observations of spectrophotometric standard stars. Further corrections for atmospheric extinction were applied using tabulated extinction coefficients for each telescope site (in the pipeline archive).

The quality of the flux calibration was checked by comparison of synthetic *BV* and *r* photometry derived from the spectra, using the IRAF task `CALCPHOT`, with the observed photometry at comparable epochs. Calibrated spectra were finally dereddened for the total line-of-sight extinction and then corrected for the heliocentric velocity of the host galaxy (see Table 1).

5.2 Data analysis

The time evolution of the optical spectrum of SN 2012ec, obtained from 8 to 161 d, is shown in Fig. 7 and corresponding line identifications are presented in Fig. 8. Fig. 9 shows the evolution of the velocities of H_α, H_β, Fe II (5018 Å) and Fe II (5169 Å) for SN 2012ec. A list of line velocities is presented in Table 8.

[5] Fast reduction data are available on WISeREP (Yaron & Gal-Yam 2012) and full reduced data can be accessed from the ESO Phase 3 archive; all details on www.pessto.org

Spectra at early phases show a blue continuum, broad Balmer lines and He I at 5876 Å. Lines show the typical P-Cygni profile, from which we estimate expansion velocities from the measurement of the position of the minimum of the absorption component. At early times, the estimated velocities are 12 200 ± 150 km s^{-1} for H_α, 11 000 ± 150 km s^{-1} for H_β and 10 500 ± 150 km s^{-1} for He I. A blackbody fit to the continuum of these spectra, in the range 4000–9500 Å yielded a temperature 11 900 ± 900 K.

Spectra from day 21 to 44 show, in addition to the Balmer lines, some iron-group elements like Fe II (4629 Å), Fe II (5018 Å), Fe II (5169 Å) and Sc II (6246 Å). There is also a feature at 8200 Å due to the Ca II infrared triplet. The H_α velocity decreases to 10 000 ± 120 km s^{-1}, H_β to 9000 ± 120 km s^{-1}, while the velocities for the Fe II (5018 Å) and Fe II (5169 Å) were measured to be ∼6000 ± 100 km s^{-1}. The temperatures derived from blackbody fits to the continuum show a decrease from 8000 ± 500 K to 6000 ± 300 K.

Spectra from day 49 to 138 show the appearance of lines due to other heavy elements, such as Ba II (5981 Å), Ba II (6142 Å), Ti II (4100 Å), and numerous blends of Fe II lines, while the absorption feature of Na ID is no longer visible. At early times, the Na ID feature is clearly visible as an absorption on the continuum, but at later times it is blended with complex broad features. At these phases the velocities decrease for all elements: the velocity of H_α decreases to 5000 ± 90 km s^{-1} and Fe II (5018 Å) and Fe II (5169 Å) decrease to 2000 ± 120 km s^{-1}. The presence of the iron-group line blends prevents the detection of H_β. A fit to the continuum yields a temperature of 5000 ± 400 K.

At late times, the spectrum at 161 d shows forbidden [O I] lines (6300, 6364 Å) and the semiforbidden Ca II] doublet (7291, 7394 Å).

The ejecta velocities of SN 2012ec have been compared with those measured for other Type II-P SNe: SN 2012A, SN 2012aw, SN 2004et and SN 1999em (see Table 9). At early phases, the H_α velocity is lower than that estimated for SN 2012aw (∼14 000 km s^{-1}; Dall'Ora et al. 2014), but higher than the one estimated for SN 2012A (∼10 200 km s^{-1}; Tomasella et al. 2013), and comparable with the one of SN 1999em (∼12 000 km s^{-1}; Elmhamdi et al. 2003a). At later phases (40 d), the Fe II (5169 Å) velocities are higher than those estimated for SN 2012A (∼3500 km s^{-1}), comparable with those of SN 2004et (∼4000 km s^{-1}) and SN 1999em (∼4200 km s^{-1}), but they are still lower than that of SN 2012aw (∼5500 km s^{-1}). In summary, the ejecta velocities measured for SN 2012ec velocities are similar to those measured for SNe 1999em and 2004et, but are consistently lower than for SN 2012aw and higher than for SN 2012A. We also point out that the evolution of the Fe II (5169), H_α and H_β velocities of SN 2012ec are in excellent agreement with the trends shown in fig. 16 of Faran et al. (2014), based on a sample of 23 well-studied II-P SNe.

A close-up showing the time evolution of the H_α, H_β and Ca II line profiles for SN 2012ec is shown in Fig. 10.

The NIR spectra cover the period from day 21 to 161 (Fig. 11). The H I Paschen lines are clearly visible at all epochs. Starting from day 68 we identify also He I and Ca I lines and Br_γ. The elements identified in the NIR spectra (Fig. 8) are typical of Type II-P SNe, in particular the spectra at 71 and 79 d are similar to the NIR spectrum of SN 2012A at 72 d (Tomasella et al. 2013).

6 HYDRODYNAMIC MODELLING

To constrain the main physical properties of the progenitor and the energetics of the explosion, we performed hydrodynamical

Table 7. Summary of instrumental setups used for the spectroscopic follow-up campaign.

Telescope	Instrument	Grism	Range (Å)	Resolution (Å)	# of epochs
NTT (3.58m)	EFOSC2	Gr11, Gr16	3350–10 000	12	10
NTT (3.58m)	SOFI	GB	9400–14 000	20	7
NTT (3.58m)	SOFI	GB, GR	14 000–25 000	20	3
CAO (1.82m)	AFOSC	Gr4	3500–8200	24	3
Pennar (1.22m)	B&C	Gr300	3400–7800	10	2
NOT (2.56m)	ALFOSC	Gr4	3400–9000	14	1
WHT (4.2m)	ISIS	R300B+R158R	3500–10 000	5	1
ANU (2.3m)	WiFeS	B+R	3300–9000	2	2

NTT = New Technology Telescope with the optical camera EFOSC2 and with the NIR camera SOFI; CAO = the Copernico telescope at Asiago Observatory with AFOSC; Pennar = Galileo telescope at Asiago Observatory with the B&C spectrograph; NOT = Nordic Optical Telescope with ALFOSC; WHT = William Herschel Telescope with ISIS; ANU = Australian National University telescope with WiFeS.

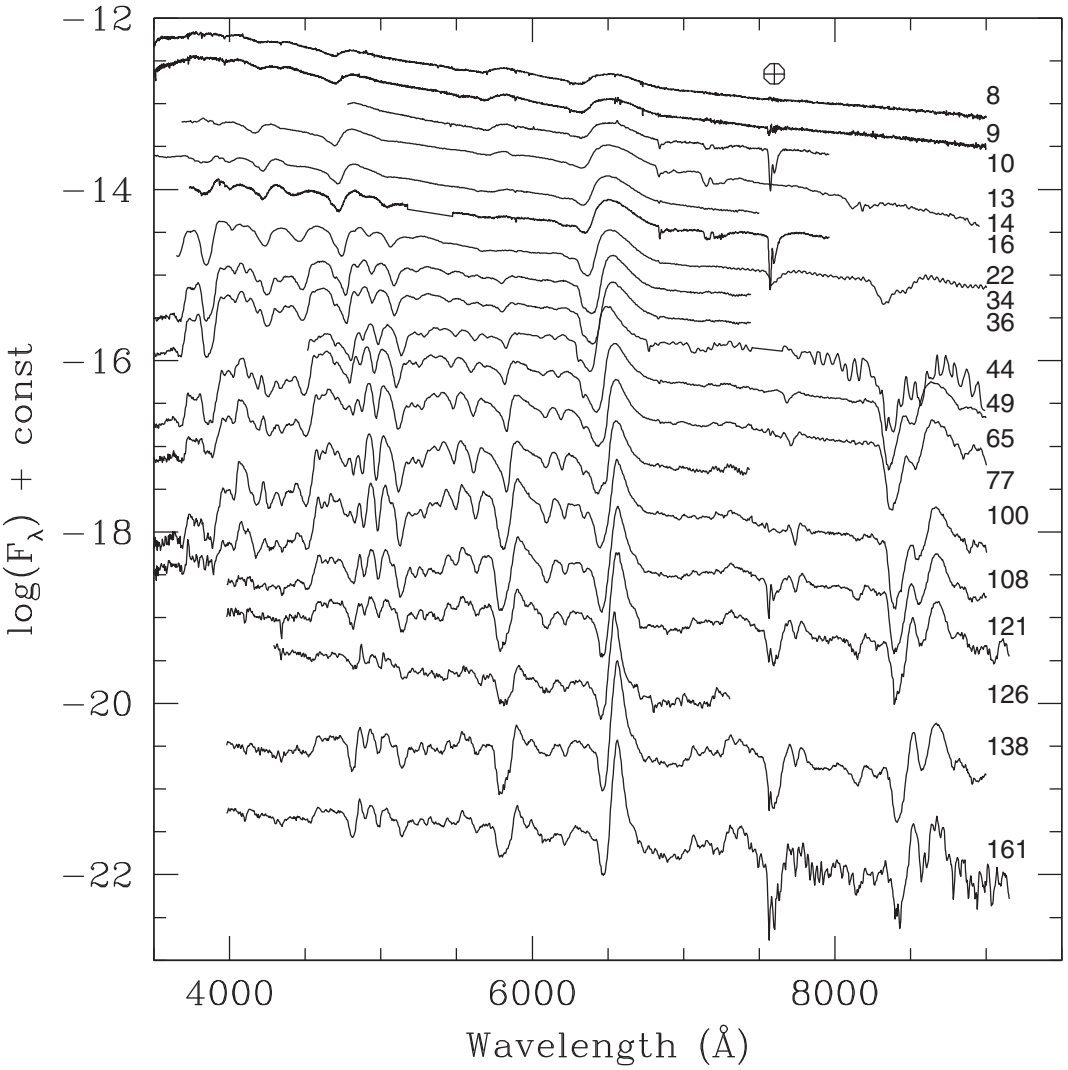

Figure 7. The optical spectroscopic evolution of SN 2012ec during the photosperic phase, from +8 to +161 d.

modelling of SN 2012ec. Among the most important parameters we need to constrain are the ejected mass, the radius of the progenitor, the explosion energy and the ejected ^{56}Ni mass (Zampieri et al. 2003; Kasen & Woosley 2009). These were found by comparing the observed bolometric luminosity, the evolution of line velocities and continuum temperature at the photosphere with the corresponding simulated quantities (Zampieri et al. 2003; Pumo et al. 2010). The comparison procedure consists of performing a simultaneous χ^2 fit of all the relevant observables against those predicted by the model calculations. This approach was successfully adopted for other

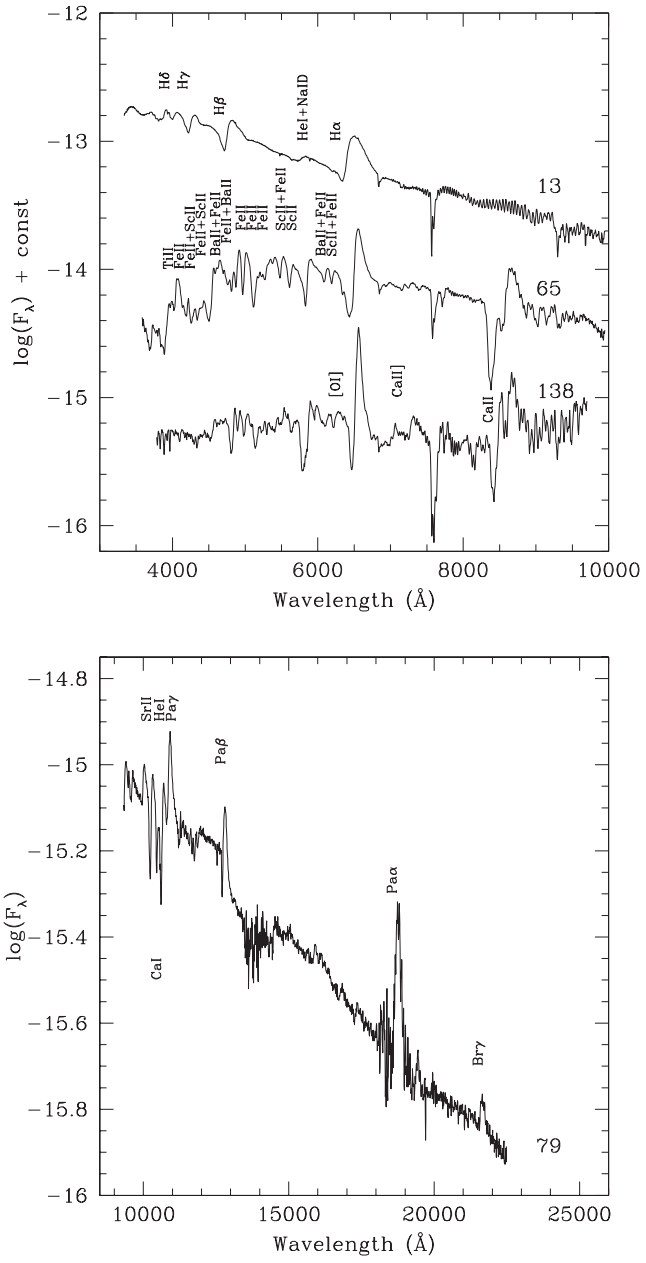

Figure 8. Identifications of line features observed in optical (at three characteristic epochs; top panel) and NIR spectra (bottom panel) of SN 2012ec.

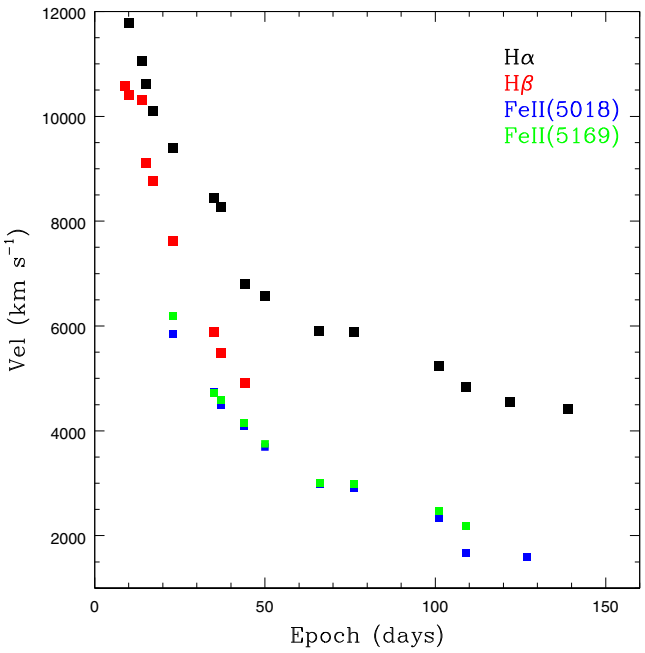

Figure 9. Ejecta velocity evolution, estimated from the H_α, H_β, Fe II (5018 Å) and Fe II (5169 Å) lines.

CC-SNe (e.g. SN 2007od, Inserra et al. 2011; SN 2009bw, Inserra et al. 2012; SN 2009E, Pastorello et al. 2012; SN 2012A, Tomasella et al. 2013; and SN 2012aw, Dall'Ora et al. 2014).

The hydrodynamical modelling of the explosion was performed with two different codes: a semi-analytic code (Zampieri et al. 2003) that solves the energy balance equation for a constant density envelope which expands homologously; and a radiation-hydrodynamics code (Pumo & Zampieri 2011) that can simulate the full radiative-hydrodynamical evolution of the ejected material. The latter code solves the hydrodynamic equations of a self-gravitating, relativistic fluid interacting with radiation, and incorporates an accurate treatment of radiative transfer and of the evolution of the ejected material, considering both the gravitational effect of the compact remnant and the heating effects related to the decays of radioactive isotopes synthesized during the CC-SN explosion. The first code is used to investigate the more likely parameter space and provide a robust, first estimate of the best-fitting model. A more detailed and time-consuming search is then performed with the radiation-hydrodynamics code. This modelling is appropriate only if the emission from the CC-SN is dominated by freely expanding ejecta. Clearly, interaction with the circumstellar medium can affect the early evolution of the light curve in a way not presently predicted by the models.

An extended grid of semi-analytic models was computed, covering a wide range in mass. The χ^2 distribution of the models as a function of ejected mass is shown in Fig. 12 and shows two comparable minima, one at $\sim$9.1 $M_\odot$, the other at $\sim$12.6 $M_\odot$. The best-fitting model corresponding to the first minimum (9.1 $\pm$ 0.8 $M_\odot$) has an initial radius of $\sim 2.3 \times 10^{13} \pm 0.7$ cm (330 $\pm$ 100 $R_\odot$), a total explosion energy of $\sim 0.7 \pm 0.2$ foe and an ejected ^{56}Ni mass of $\sim$0.035 $M_\odot$. The model corresponding to the second minimum has an initial radius of $1.6 \pm 0.5 \times 10^{13}$ cm (230 $\pm$ 70 $R_\odot$), a total explosion energy of 1.2 $\pm$ 0.4 foe and an ejected ^{56}Ni mass of $\sim$0.035 $M_\odot$. In light of the results of the progenitor detection in pre-explosion observations, we only consider the 'high-mass' minimum further. The best-fitting model corresponding to the second minimum is shown in Fig. 13 and appears to be in good agreement with all the observables.

7 HOMOGENEOUS COMPARISON WITH THE TWO WELL-STUDIED II-P SNe 2012A AND 2012AW

In this section, we present a detailed comparison of SN 2012ec with two well-studied Type II-P SNe: 2012A and 2012aw. In all three cases, a progenitor was detected in pre-explosion images and sufficient photometric and spectroscopic observations were available to permit a homogenous analysis of the properties of the SNe using the same hydrodynamical code. SN 2012ec was discovered 9 d after the explosion, while the other SNe were discovered much sooner after

Table 8. Measured expansion velocities (from the minima of P-Cygni absorption) for SN 2012ec. Estimated uncertainties are in parentheses.

Date	MJD	Epoch[a] (d)	H_α (km s^{-1})	H_β (km s^{-1})	Fe II (5018) (km s^{-1})	Fe II (5169) (km s^{-1})	Sc II (5533) (km s^{-1})	Ca II (8520) (km s^{-1})
20120812	56152	8	12 200 (150)	10 600 (150)				
20120813	56153	9	11 800 (130)	10 400 (150)				
20120817	56157	13	11 000 (160)	10 300 (130)				
20120818	56158	14	10 600 (120)	9100 (120)				
20120820	56160	16	10 100 (120)	8800 (110)				
20120826	56166	22	9400 (100)	7600 (120)	5800 (100)	6200 (100)		
20120907	56178	34	8400 (110)	5900 (110)	4700 (100)	4700 (120)	5000 (120)	
20120909	56180	36	8300 (110)	5500 (130)	4500 (110)	4600 (100)	4600 (130)	
20120916	56187	43	6800 (120)	4900 (110)	4100 (110)	4100 (130)		
20120922	56193	49	6600 (110)		3700 (100)	3700 (100)	3800 (140)	5600 (120)
20121008	56209	56	5900 (110)		3000 (100)	3000 (140)	3100 (100)	4900 (140)
20121017	56219	75	5800 (170)		2900 (110)	2900 (150)		
20121112	56244	100	5230 (120)		2300 (120)	2400 (100)	2100 (130)	4100 (100)
20121122	56252	108	4800 (100)			2200 (100)	2000 (150)	3700 (150)
20121203	56265	121	4500 (100)		2000 (110)			3600 (130)
20121212	56270	126			1600 (100)			
20121220	56282	138	4400 (100)					3500 (140)

[a]Epoch from the explosion.

Table 9. Expansion velocity of SN 2012ec at selected epochs, compared to other Type II-P SNe.

	2012aw	2012ec	1999em	2004et	2012A
$H\alpha$ (∼10 d)	14 000	12 200	12 000		10 200
Fe II (∼40 d)	5500	4100	4200	4000	3500
Fe II (∼100 d)	3000	2400	2000	2000	2000

explosion (see Table 10). SN 2012aw was discovered in M95 at a distance modulus $\mu = 29.96 \pm 0.04$ mag and with a total reddening of $E(B-V) = 0.086$ mag; while SN 2012A was discovered in NGC 3239 at $\mu = 29.96 \pm 0.15$ and $E(B-V) = 0.037$ mag.

The estimates of the initial masses of the progenitors, through direct detection of the precursor, were: $M_{12aw} = 14$–$26\,M_\odot$ (Fraser et al. 2012), M_{12ec} in the range 14–22 $M_\odot$ (Maund et al. 2013) and $M_{12A} = 8$–$15\,M_\odot$ (Tomasella et al. 2013). In a separate analysis of the pre-explosion observations of SN 2012aw, Van Dyk et al. (2012) reported an initial mass of 15–20 $M_\odot$. A major uncertainty in estimating the progenitor mass is degeneracy between temperature and reddening. Kochanek et al. (2012) showed that a different treatment of the extinction results in a luminosity of $\log(L/L_\odot) = 4.8$–5.0, corresponding to a progenitor main sequence mass of 13–16 $M_\odot$ (Jerkstrand et al. 2014b), which is in agreement with the nebular spectral modelling and the amount of oxygen produced by SN 2012aw.

Fig. 14 shows the photometric evolution of the absolute magnitudes in the *R* and *V* bands of SN 2012ec, SN 2012aw and SN 2012A. We note that SN 2012ec is intermediate between the more luminous SN 2012aw and the fainter SN 2012A. The duration of the plateau and the post-plateau decline is longer in SN 2012aw and shorter and steeper in SN 2012A. Again, SN 2012ec shows an intermediate behaviour, with quite a short plateau and a slower post-plateau drop. The absolute magnitude in the *R* band for these SNe, on the plateau (∼ 60 d), were $M_R(12aw) = -17.1$ mag, $M_R(12ec) = -16.7$ mag and $M_R(12A) = -16.2$ mag.

A comparison of the colour evolution of SN 2012ec with SN 2012aw and SN 2012A is shown in Fig. 15. The colour of each SN has been corrected for reddening for a proper comparison. The colour evolution of SN 2012ec has already been discussed in Section 4.2. From Fig. 15, we can see that the colour evolution of SN 2012ec is similar to that of the other two SNe.

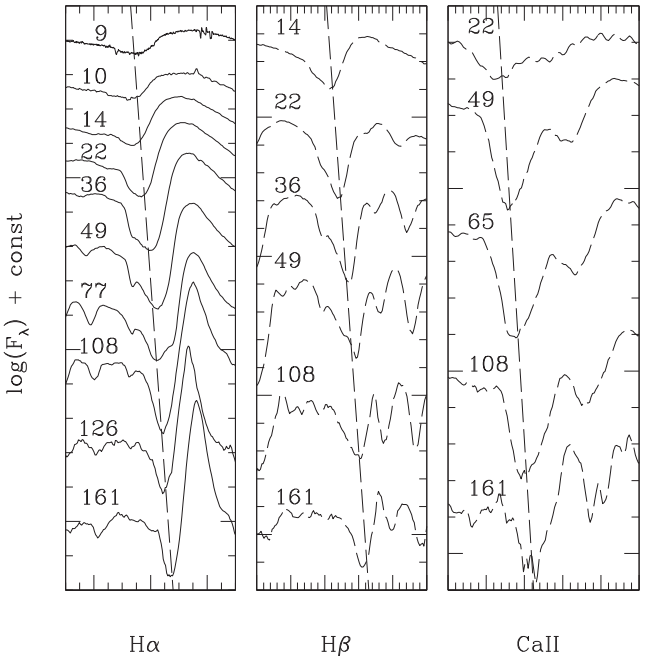

Figure 10. Time evolution of H_α, H_β and Ca II NIR triplet for SN 2012ec.

Fig. 16 shows a comparison of the bolometric light curves of SNe 2012ec, 2012A and 2012aw, where SN 2012ec is of intermediate luminosity between the other two SNe. In particular, during the plateau phase, SN 2012ec is more luminous than SN 2012A and exhibits a longer plateau. Conversely, SN 2012aw is clearly of higher luminosity than SN 2012ec throughout the entirety of the

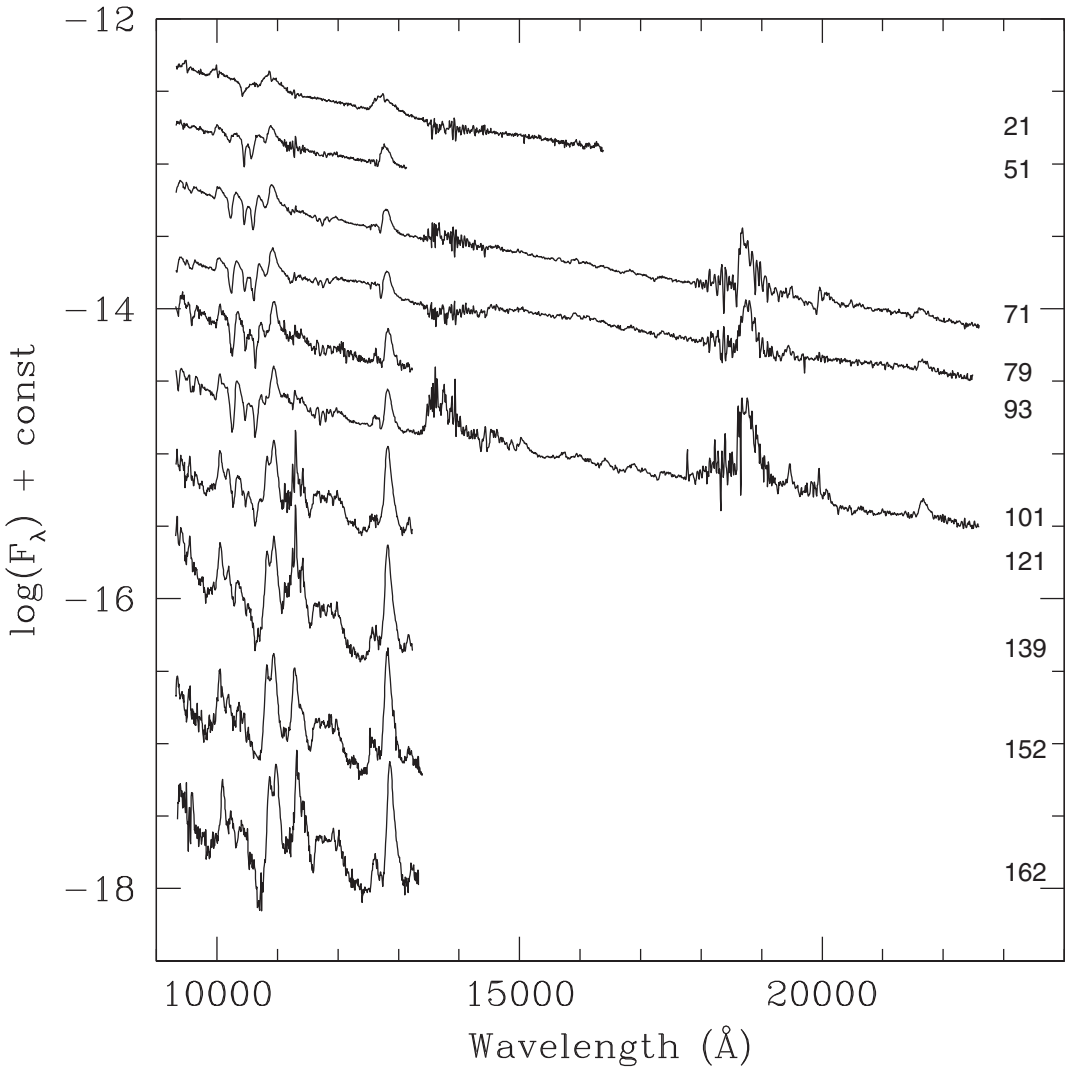

Figure 11. NIR spectroscopic evolution of SN 2012ec. Individual spectra have been shifted in flux for clarity. Numbers on the right indicate the epochs from explosion.

photospheric phase and has a longer plateau of ∼100 d (Dall'Ora et al. 2014).

From the comparison of the ^{56}Ni masses estimated for the three SNe, we may note a sequence in the values: $M(^{56}\mathrm{Ni})_{12aw} = 0.056 \pm 0.013\,\mathrm{M}_\odot$, $M(^{56}\mathrm{Ni})_{12ec} = 0.040 \pm 0.015\,\mathrm{M}_\odot$ and $M(^{56}\mathrm{Ni})_{12A} = 0.011 \pm 0.004\,\mathrm{M}_\odot$.

In Fig. 17, we show a comparison of the spectra of SN 2012ec with those of SN 2012aw and SN 2012A at three different epochs, highlighting the spectroscopic similarities between the three SNe at all epochs.

We also compared the ejecta velocities measured from H_α and Fe II (5169 Å) for SN 2012ec with the velocities measured for other Type II-P SNe (see Fig. 18). SN 2012aw has an initial H_α velocity ∼14 000 km s^{-1}, higher than measured for SN 2012ec (∼12 200 km s^{-1}) and for SN 2012A (∼10 200 km s^{-1}). After 100 d, the velocity of H_α decreases to ∼6000 km s^{-1} for SN 2012aw, which is still higher than measured for SN 2012ec (∼5000 km s^{-1}) and for SN 2012A (∼5000 km s^{-1}). The initial Fe II (5169 Å) of SN 2012aw is ∼6500 km s^{-1}, still higher than those of SN 2012ec (∼6000 km s^{-1}) and of SN 2012A (∼5200 km s^{-1}). After ∼100 d it drops to ∼3000 km s^{-1} for SN 2012aw, to ∼2500 km s^{-1} for SN 2012ec and to ∼2000 km s^{-1} for SN 2012A. In terms of ejecta velocities, SN 2012ec is intermediate between SN 2012aw and SN 2012A.

A comparison of the temperature estimated via blackbody fitting of the SED evolution for the three SNe is presented in Fig. 19, from which it is clear that the temperature evolutions of SN 2012ec and SN 2012A are similar, and significantly hotter than SN 2012aw (from ∼20–30 d post-explosion).

The ejected mass calculated for SN 2012ec is 12.6 $\mathrm{M}_\odot$, which is comparable to the value estimated for SN 2012A (12.5 $\mathrm{M}_\odot$; Tomasella et al. 2013), but lower than value calculated for SN 2012aw (20 $\mathrm{M}_\odot$; Dall'Ora et al. 2014). Similarly the initial radius for SN 2012ec is comparable to SN 2012A (∼260 $\mathrm{R}_\odot$), but smaller than for SN 2012aw (∼400 $\mathrm{R}_\odot$). Conversely, the estimated energy of SN 2012ec of 1.2 foe is higher than the value estimated for SN 2012A (0.48 foe) but similar to the energy of SN 2012aw (1.5 foe).

In summary, SN 2012ec is more luminous than SN 2012A, synthesized more ^{56}Ni and has higher expansion velocities. The ejecta masses of the two SNe are comparable, but the pre-SN radius and the masses of the progenitors are slightly different. This indicates that the progenitor of SN 2012ec progenitor was likely to be more

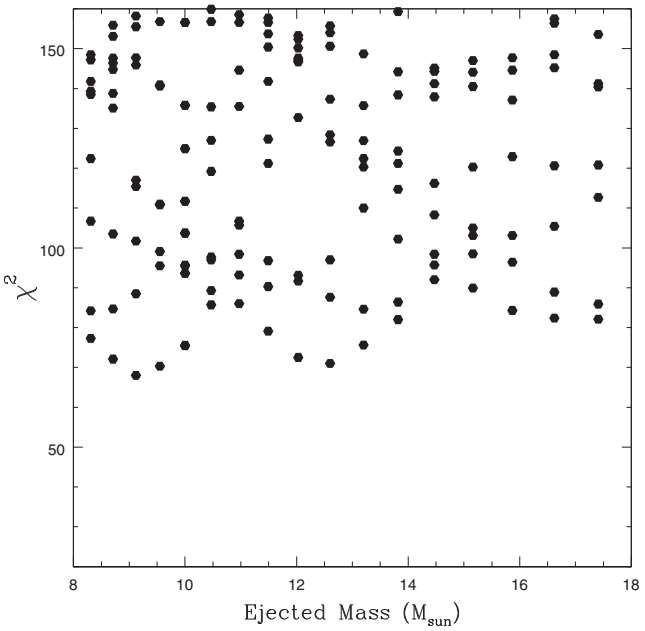

Figure 12. χ^2 distribution of the fit of the semi-analytical model to the observed quantities, as a function of the estimated ejected mass.

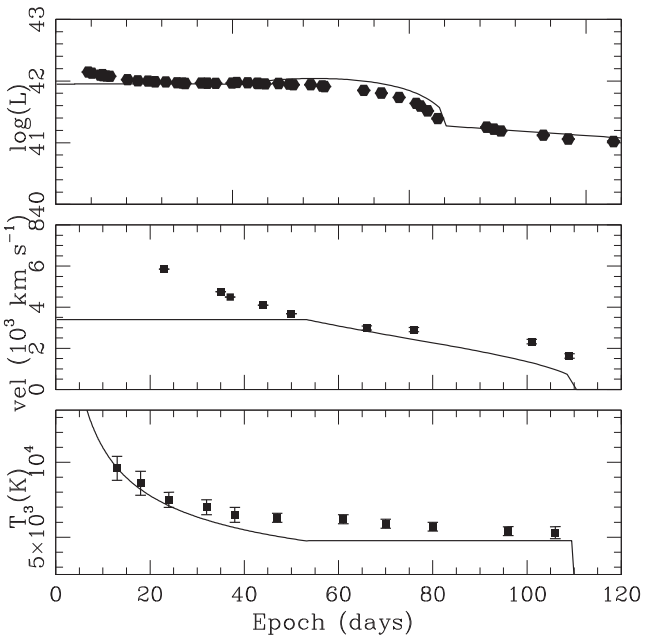

Figure 13. Time evolution of the main observables of SN 2012ec (filled dots), compared to the 'high-mass' best-fitting model (solid line). The top panel shows the fit of the bolometric light curve; the middle panel shows the fit of the Fe II velocity and the bottom panel shows the fit of the continuum temperature.

massive, but more compact the progenitor of SN 2012A. SN 2012aw has a larger initial radius, a more massive envelope and more energetic explosion that produced more ^{56}Ni and higher ejecta velocities than SN 2012ec. It is interesting to compare these estimates with the analysis of Poznanski (2013), who suggests a simple scaling relation between the energy deposited in the exploding core and the mass of the progenitor that, in turn, reflects on a linear correlation

Table 10. Comparison of the main parameters of SNe 2012ec, 2012aw and 2012A.

	SN 2012aw	SN 2012ec	SN 2012A
μ (mag)	29.96	31.19	29.96
$E(B-V)$ (mag)	0.086	0.124	0.037
MJD_{expl} (d)	56002	56151	55933
MJD_{disc} (d)	56003	56143	55934
$v_{Fe\,II}$ (km s^{-1})[a]	∼4200	∼3700	∼2800
M_R (mag)	−17.1	−16.7	−16.2
$L(10^{42}$erg s$^{-1})$[b]	1.1	0.9	0.5
Plateau duration (d)	100	90	80
^{56}Ni ($M_\odot$)	0.056	0.040	0.011
E (foe)[c]	1.5	1.2	0.48
R (10^{13} cm)	3	1.6	1.8
M_{eject} ($M_\odot$)	20	12.6	12.5
M_{prog} ($M_\odot$)[d]	13–16	14–22	8–15

[a]At ∼50 d.
[b]At the plateau.
[c]1 foe= 10^{51} erg.
[d]Mass of the progenitor as estimated from the pre-explosion images.

between mass and ejecta velocity. In particular, the positions of the ejected masses from the hydrodynamical code of SN 2012A and SN 2012aw in the Fig. 1 of Poznanski (2013) are consistent with a steeper law $M \propto v^{1.5}$, while the ejected mass for SN 2012ec is much lower than expected from both the $M \propto v$ and $M \propto v^{1.5}$ relations. Since the hydrodynamical code estimates the ejecta masses, and not the progenitor masses, for SN 2012ec the discrepancy could be explained with a very efficient mass-loss mechanism. Unfortunately, the same argument cannot be invoked for SN 2012A and SN 2012aw. We also note that the Poznanski (2013) analysis was based on progenitor masses estimated from stellar evolution models, which are based on a different input physics than the hydrodynamical codes.

The main characteristics of the comparisons between the three SNe are summarized in Table 10.

8 TYPE II-P SNe AS STANDARD CANDLES

The extragalactic distance scale is intimately connected with Type Ia SNe, up to cosmological distances, and through Type Ia SNe the acceleration of the Universe was discovered (Riess et al. 1998; Schmidt, Suntzeff & Phillips 1998; Perlmutter et al. 1999). At the present time, current facilities allow us to detect and study Type Ia SNe up to $z = 1.7$ (Rubin et al. 2013), while the next generation of extremely large telescopes will allow us to study Type Ia SNe up to $z \sim 4$ (Hook 2013). At high z, however, the number of Type Ia SNe may significantly decrease, due to the long lifetimes of their progenitors. Alternatively, the ubiquitous Type II (CC) SNe could be an appealing choice to probe further cosmological distances. While Type Ia SNe are the product of an old to intermediate stellar population, Type II SNe come essentially from a young stellar population, and thus constitute a homogeneous sample with respect to the age of the stellar population. It should also be noted, however, that Type II SNe are significantly fainter than Type Ia SNe and that they explode in younger and dustier regions, making their discovery and study more difficult.

Although the characteristics of the light curves of the Type II SNe (peak luminosity, decline rate, presence and duration of the plateau) span a broad range of values, their use as distance indicators was

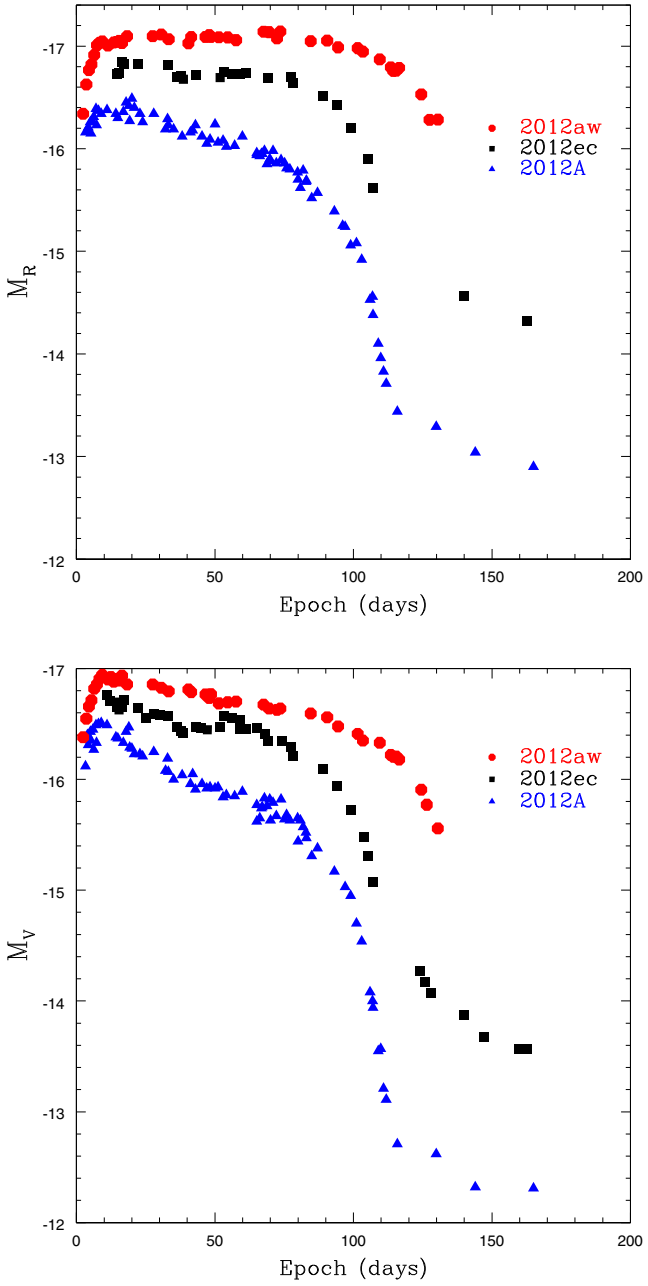

Figure 14. Comparison of the light curves in the R (top panel) and V (bottom panel) bands of SN 2012ec, with SN 2012aw and SN 2012A.

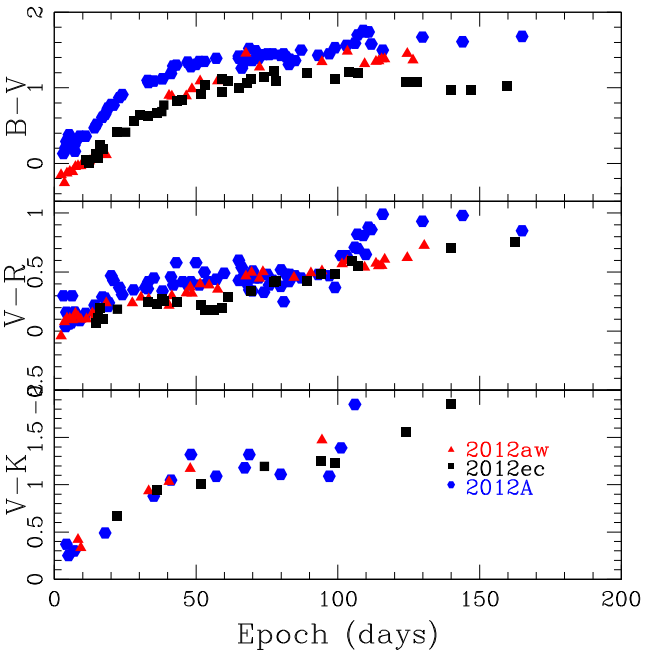

Figure 15. Comparison of the colour evolution of SN 2012ec, in the $B-V$ (top panel), $V-R$ (middle panel) and $V-K$ (bottom panel), with SN 2012aw and SN 2012A.

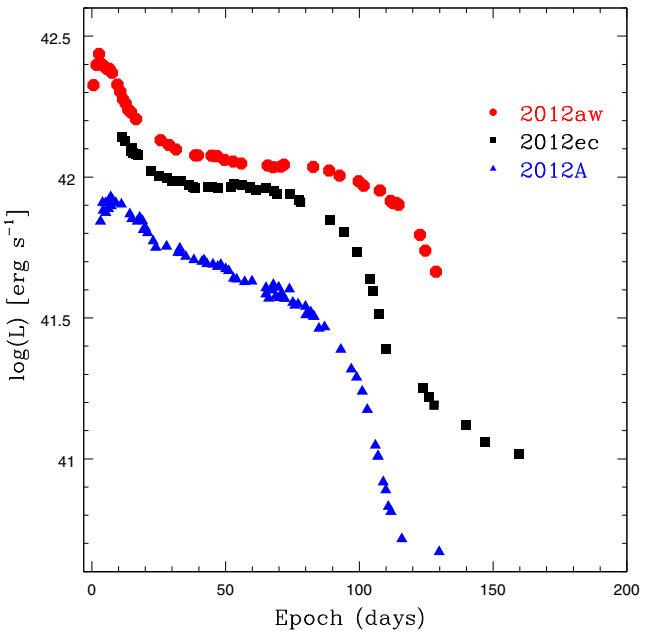

Figure 16. Pseudo-bolometric light curve of SN 2012ec, compared to SN 2012aw and SN 2012A.

already recognized by Kirshner & Kwan (1974), who applied the Baade–Wesselink analysis to SN 1969L and SN 1970G through the expanding photosphere method (EPM), and by Mitchell et al. (2002), who modified the EPM method by introducing spectral synthesis analysis (Spectral-fitting Expanding Atmosphere Method, SEAM). Subsequently, Dessart & Hillier (2005) further exploited the EPM method by applying non-LTE atmospheric models. Both EPM and SEAM methods have been successfully applied to SNe at cosmological distances (e.g. Schmidt, Kirshner & Eastman 1994; Baron et al. 2004), but require well sampled light curves and high-quality spectra.

More specifically, for Type II-P SNe, Hamuy & Pinto (2002) found a tight empirical correlation between the bolometric luminosity and the expansion velocity of the ejecta during the plateau phase. The luminosity and the expansion velocity (as measured from the Fe II (5169 Å) line) are estimated at approximately the 'half plateau' phase, conventionally set at 50 d. This method, dubbed the 'standardized candle method', was subsequently investigated by Nugent et al. (2006), Poznanski et al. (2009), D'Andrea et al. (2010) and Olivares et al. (2010), with the advantage that it requires less input data than both EPM and SEAM methods. The empirical correlation at the base of the SCM was theoretically reproduced by Kasen & Woosley (2009), who pointed out that the correlation relies on the simple behaviour of the expanding hydrogen envelope. They also

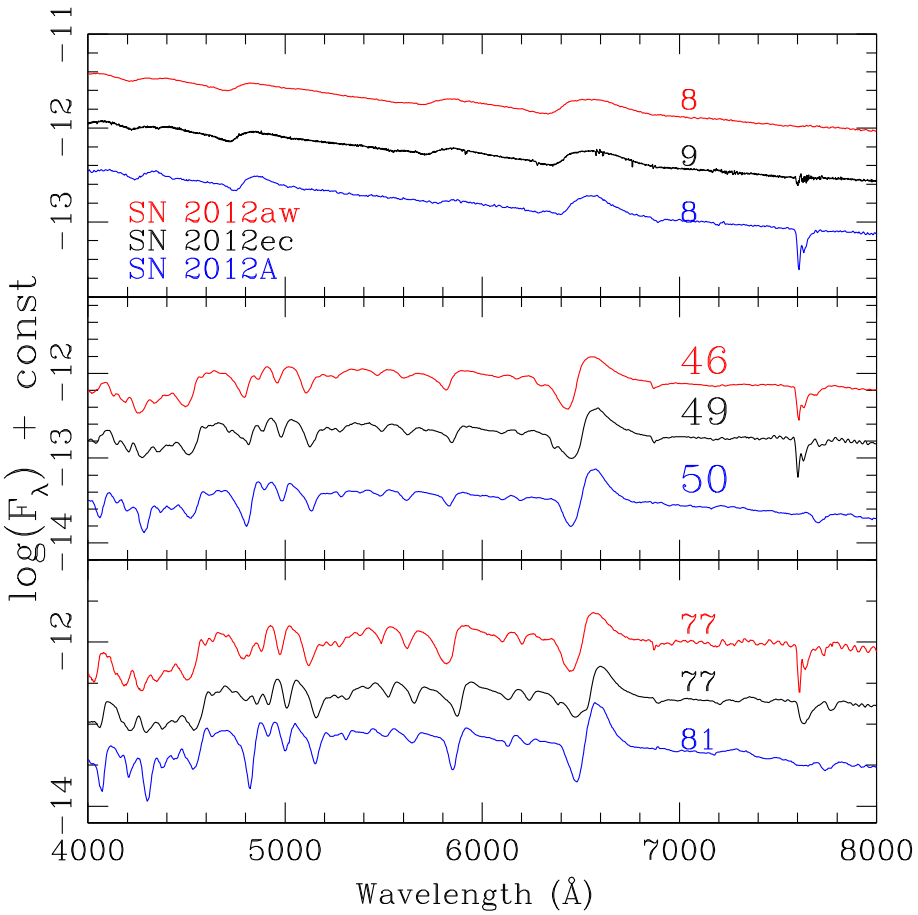

Figure 17. Comparison of the spectra of SN 2012ec, SN 2012aw and SN 2012A at three different epochs, i.e. at early times, during the plateau phase and at the end of the plateau.

warned, however, that the SCM may be sensitive to the progenitor metallicity and mass, which in turn could lead to systematic effects.

Almost all the quoted calibrations adopt 50 d post-explosion as a reference phase that roughly corresponds to the 'half-plateau'. Other choices for the reference phase during the plateau phase can be set, but with the *caveat* that the velocity measured from the Fe II (5169 Å) line is moderately decreasing over the duration of the plateau and that the method requires knowledge of the epoch of the explosion. Only Olivares et al. (2010) adopted a 'custom' reference phase for each SN, due to the fact that the length of the plateau varies from SN to SN. For this reason, they suggested adopting a reference epoch 30 d prior to the epoch at which the light curve has declined to a brightness midway between the plateau brightness and the brightness at which it joins the radioactive tail.

In this paper, we take advantage of the homogeneous analysis of the three Type II-P SNe (SNe 2012ec, 2012aw and 2012A) to perform a detailed comparison of the available calibrations of SCM and assess the robustness of the method. More specifically, for the comparison we adopt the *I*-band calibrations of SCM, namely: equation 2 of Hamuy & Pinto (2002); equation 1 of Nugent et al. (2006); equation 2 of Poznanski et al. (2009); equation 2 of D'Andrea et al. (2010);[6] and equation 16 of Olivares et al. (2010). Our estimated distances to the three SNe are compared with a homogeneous set of distances, based on primary (Cepheids, tip of the red giant branch or TRGB) and secondary distance indicators (Tully–Fisher, surface brightness fluctuations or SBF), available in the Extragalactic Distance Database (Tully et al. 2009). In Table 11 we report, for each SN, the distance estimated with the above calibrations. Moreover, we show the difference between the SCM distance and the estimates from the primary (when available) and secondary distance indicators. Finally, for each calibration, we report the mean difference and dispersion of the SCM distances with the estimates based on the primary and secondary distance indicators. The studied sample follows the Hamuy & Pinto (2002) relation with a good agreement as shown in Fig. 20.

Table 11 may suggest that the Hamuy & Pinto (2002) calibration gives more homogenous results with respect to other calibrations. However, it must be noted that our test is based on only three SNe and that all the calibrations are consistent within the errors. We note that the Hamuy & Pinto (2002) calibration was derived assuming a value of $H_0 = 65$ km s^{-1} Mpc^{-1}, significantly lower than the estimate of $H_0 = 73.8 \pm 2.4$ km s^{-1} Mpc^{-1} of Riess et al. (2011), but in agreement with $H_0 = 63.7 \pm 2.3$ km s^{-1} Mpc^{-1} given by Tammann & Reindl (2013). The large scatter in the Olivares et al. (2010) calibration could be due to the difficulty in estimating the reference phase, when a well sampled light curve covering the end of the plateau, is not available. All these calibrations rely on moderately distant SNe, embedded in the Hubble flow or for which SBF distances are available. However, these distances could still be

[6] In passing, we note that the Poznanski, Nugent & Filippenko (2010) recalibration of this work led to a Hubble diagram with a scatter of only 11 per cent.

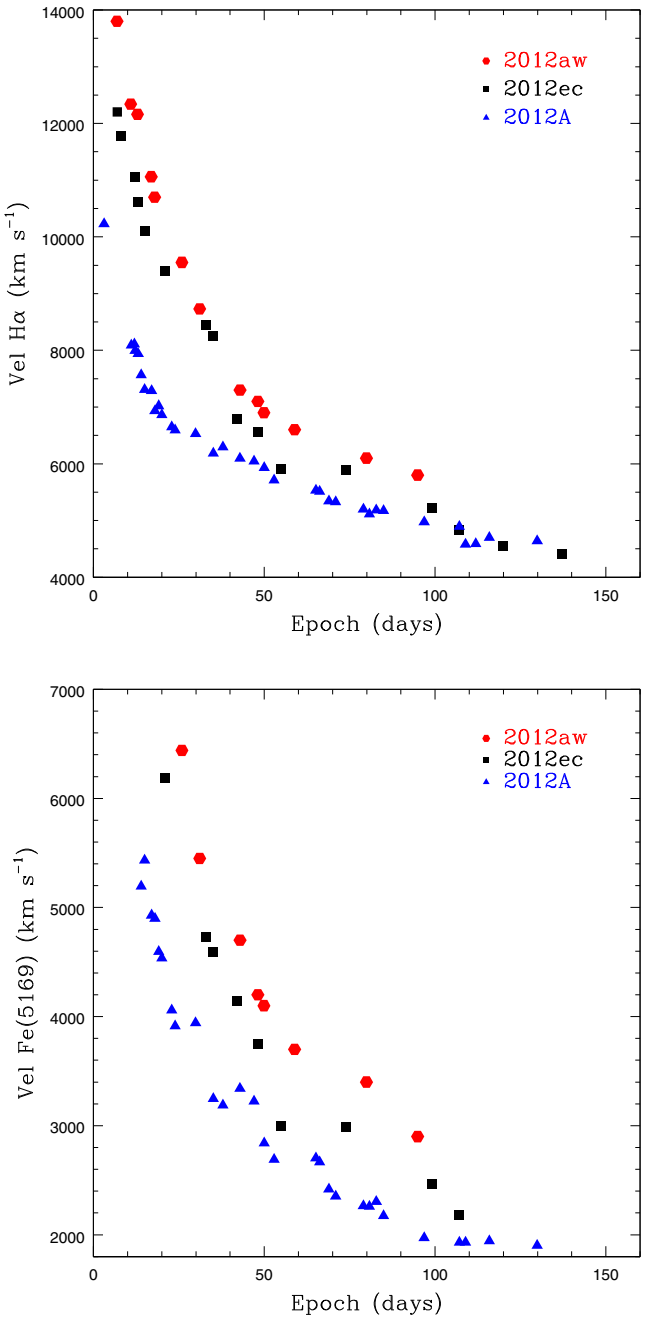

Figure 18. Comparison of the ejecta velocities of SN 2012ec, SN 2012A and SN 2012aw, measured from the H_α (top panel) and Fe II (5169 Å) lines (bottom panel).

affected by systematics not completely understood. For these reasons a new calibration of the SCM, based on nearby Type II-P SNe for which primary (Cepheids and TRGB) and homogenous secondary indicators (TRGB) distances are available, would be of great interest. Moreover, for these SNe the metallicity effects suggested by Kasen & Woosley (2009) could also be investigated. The average of the five individual estimates of the distances for SN 2012ec gives a distance modulus of 31.22 ± 0.08 mag, which we adopt as our final SCM-based distance. This value is in excellent agreement with the Tully–Fisher distance of 31.19 ± 0.13, adopted for our analysis.

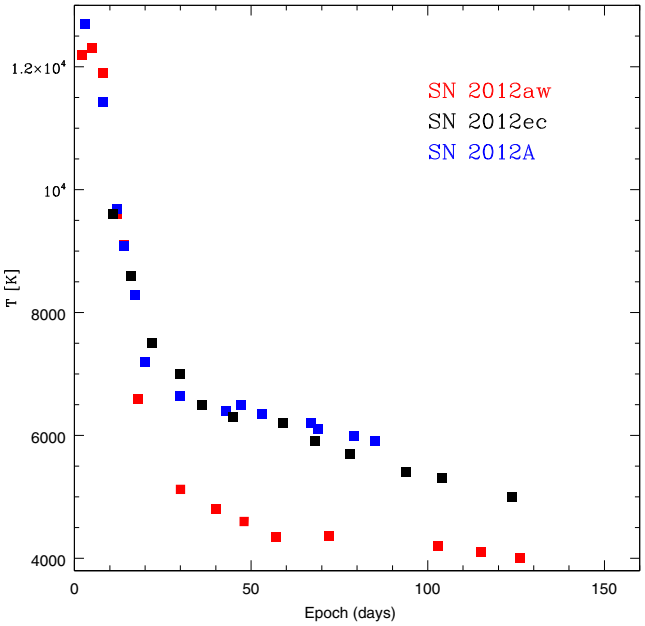

Figure 19. Comparison of the time evolution of the photospheric temperatures of SNe 2012ec, 2012A and 2012aw.

9 CONCLUSIONS

We have presented the results of the Large Programme 'Supernova Variety and Nucleosynthesis Yelds' and PESSTO photometric and spectroscopic monitoring campaign of SN 2012ec. This is one of the most intensively observed and well-investigated Type II-P SNe to date. The optical and spectroscopic monitoring during the photospheric phase lasted for ∼161 d and allowed us to determine the evolution of the pseudo-bolometric luminosity, the expansion velocity and the photospheric temperature and ^{56}Ni mass. These parameters, analysed in conjunctions with hydrodynamical models, allowed us to estimate the explosion parameters such as the explosion energy, the envelope mass and the pre-SN radius. Correcting the data for reddening ($E(B-V) = 0.14 \pm^{+0.15}_{-0.12}$ mag) and distance modulus ($\mu = 31.19 \pm 0.13$) we estimated the luminosity to be $L = 0.9 \times 10^{42}$ erg s^{-1}, at the plateau and evaluated the ^{56}Ni mass to be $0.040 \pm 0.015\,M_\odot$. The spectra of SN 2012ec were dominated by Balmer lines in the early epochs and after 20 d the iron-group elements started to appear and become more prominent with time. The NIR spectra were dominated by Paschen lines and, starting from 68 d, it is possible to identify He I, Ca I and Br$_\gamma$. A blackbody fit to the continuum gives temperatures of 11 900 ± 900 K in the early epochs decreasing to 6200 ± 500 K at 50 d and 5000 ± 500 K in the last epochs. From the spectroscopic data set we estimate an initial velocity of 12 200 km s^{-1} for the H_α line and 11 000 km s^{-1} for H_β. The H_α velocity decreases to 5000 km s^{-1} by 50 d. At ∼25 d the iron-group elements appear, for which we measure a velocity of 6000 km s^{-1} (for Fe II). The behaviour of SN 2012ec is similar to that seen in other II-P SNe, such as SN 1999em (Elmhamdi et al. 2003a) and SN 2004et (Maguire et al. 2010).

We estimate the physical parameters of SN 2012ec through the hydrodynamical modelling described in Section 6. The fit suggests an ejected mass of $M_{\rm eject} = 12.6\,M_\odot$, a pre-SN radius of $R = 1.6 \times 10^{13}$ cm, an explosion energy of $E = 1.2$ foe and an ejected $M(^{56}{\rm Ni}) = 0.035\,M_\odot$. The progenitor mass is in agreement with independent estimate of Maund et al. (2013), $M = 14$–$22\,M_\odot$, obtained by analysing pre-explosion images and of Jerkstrand et al.

Table 11. Comparison of the SCM distances and the estimates from the primary and secondary distance indicators.

Calibration	SN	SCM (mag)	Primary (mag)	Secondary (mag)	SCM − Primary (mag)	SCM − Secondary (mag)	Mean residual (mag)
	SN 2012ec	31.22 ± 0.3		31.19		0.03	
HP2002	SN 2012aw	29.96 ± 0.3	29.96	30.00	0.00	− 0.04	0.01 ± 0.04
	SN 2012A	30.05 ± 0.3		30.00		0.05	
	SN 2012ec	31.29 ± 0.3		31.19		0.10	
Nugent06	SN 2012aw	30.03 ± 0.3	29.96	30.00	0.07	0.03	−0.03 ± 0.14
	SN 2012A	29.77 ± 0.3		30.00		− 0.23	
	SN 2012ec	31.15 ± 0.2		31.19		− 0.04	
Poznanski09	SN 2012aw	29.70 ± 0.2	29.96	30.00	− 0.26	− 0.30	−0.1 ± 0.14
	SN 2012A	30.04 ± 0.2		30.00		0.04	
	SN 2012ec	31.11 ± 0.2		31.19		− 0.08	
Olivares10	SN 2012aw	29.58 ± 0.2	29.96	30.00	− 0.38	− 0.42	−0.01 ± 0.37
	SN 2012A	30.47 ± 0.2		30.00		0.47	
	SN 2012ec	31.33 ± 0.2		31.19		0.14	
D'Andrea10	SN 2012aw	29.86 ± 0.2	29.96	30.00	− 0.10	− 0.14	0.09 ± 0.17
	SN 2012A	30.27 ± 0.2		30.00		0.27	

Notes. Quoted errors for the SCM distances are the standard deviations of the individual calibrations. The value of the distance from the primary indicators of SN 2012aw is the average from the Cepheids (Freedman et al. 2001) and the TRGB (Rizzi et al. 2007) estimates. Finally, the 'mean residual' column shows the average of the SCM − Secondary values, where the error is the standard deviation.

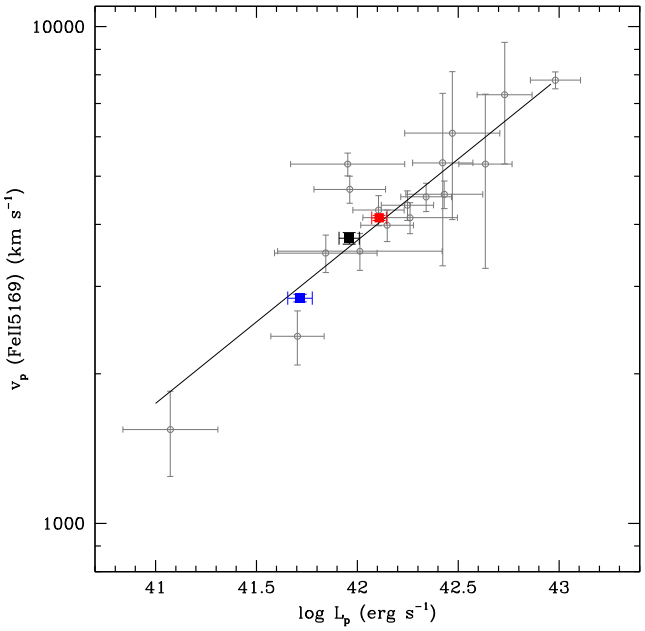

Figure 20. Our studied sample of Type II-P SNe: SN 2012ec (black), SN 2012aw (red) and SN 2012A (blue) in the original Hamuy & Pinto (2002) plane.

(2014a), $M = 13$–$15\,M_{\odot}$, obtained from modelling of the spectra in the nebular phase. Previously reported ejecta masses estimated from hydrodynamical modelling are generally too large compared to the initial mass estimated from direct detections of the progenitor on pre-explosion images (Utrobin & Chugai 2008; Maguire et al. 2010). In order to investigate this discrepancy, we performed a homogeneous comparison between three Type II-P SNe, estimating the mass of the progenitor with two different approaches. The methods and the codes used for the three objects in both cases are the same, to facilitate a reliable comparison. We analyse the bright SN 2012aw (Dall'Ora et al. 2014), the low-luminosity SN 2012A (Tomasella et al. 2013) and SN 2012ec. Several observational and derived parameters have been compared for these three objects. SN 2012aw ($M_R = -17.1$ mag, at plateau) is brighter then SN 2012ec ($M_R = -16.7$ mag), while SN 2012A is fainter ($M_R = -16.2$ mag). A comparison between the bolometric light curves shows that SN 2012ec has an intermediate luminosity between the high-luminosity SN 2012aw and the fainter SN 2012A. The nickel mass synthesized by these SNe is $M(^{56}\mathrm{Ni})_{12\mathrm{aw}} = 0.056 \pm 0.013\,M_{\odot}$, $M(^{56}\mathrm{Ni})_{12\mathrm{ec}} = 0.040 \pm 0.015\,M_{\odot}$ and $M(^{56}\mathrm{Ni})_{12\mathrm{A}} = 0.011 \pm 0.004\,M_{\odot}$. A spectroscopic comparison shows a similar time evolution at all epochs. The velocities of H_{α}, H_{β} and Fe II of SN 2012ec, place it in the middle of the higher velocities from SN 2012aw and the slowest SN 2012A at all times. The temperatures estimated are comparable for the three objects within the first 20 d, rather SN 2012ec tends to be similar to SN 2012A and they both are hotter than SN 2012aw. SN 2012aw has a more energetic explosion ($E = 1.5$ foe) than SN 2012ec and SN 2012A ($E = 0.48$ foe), but SN 2012ec is also more energetic than SN 2012A. We finally compared the results of the direct detection of the progenitors of these three SNe with the masses estimated from the hydrodynamical modelling. The progenitor mass estimated for SN 2012aw from the pre-explosion images ($M = 13$–$16\,M_{\odot}$) and from the hydrodynamical modelling ($M_{\mathrm{eject}} = 20\,M_{\odot}$) show that the two methods are not in good agreement and that SN 2012aw has a more massive progenitor then SN 2012ec, the last one having comparable ejecta mass with SN 2012A ($M = 8$–$15\,M_{\odot}$, $M_{\mathrm{eject}} = 12.5\,M_{\odot}$). The estimated initial radius of SN 2012aw ($R = 3 \times 10^{13}$ cm) indicates a larger progenitor then for SN 2012ec and SN 2012A ($R = 1.8 \times 10^{13}$ cm). The estimates of the initial radius from the hydrodynamical modelling for the three objects is lower than those from the pre-explosion images and seem to be too low for a RSG progenitor. This homogeneous analysis finds a substantial match, within the errors, of the mass of the progenitor obtained with the two methods, mitigating the discrepancy which was pointed out in previous works (Maguire et al. 2010). SN 2012ec, SN 2012aw and SN 2012A also follow the relation obtained by Hamuy & Pinto (2002). This fact, coupled with their high luminosity at UV wavelengths, make Type II-P SNe interesting probes observable with the next generation of telescopes up to high z.

ACKNOWLEDGEMENTS

We warmly thank our referee, Dovi Poznanski, for his helpful comments, which significantly improved the content and the readability of our manuscript.

We thank E. Cappellaro for the useful discussions.

CB thanks the IRAP PhD programme for the financial support. The research of JRM is supported through a Royal Society Research Fellowship. AG-Y is supported by an EU/FP7-ERC grant no [307260], 'The Quantum Universe' I-Core programme by the Israeli Committee for planning and budgeting and the ISF, GIF, Minerva, ISF and Weizmann-UK grants, and the Kimmel award. GP acknowledges partial support by proyecto interno UNAB DI-303-13/R. GP and MH acknowledge support provided by the Millennium Institute of Astrophysics (MAS) through grant IC120009 of the 'Programa Iniciativa Cientifica Milenio del Ministerio de Economia, Fomento y Turismo de Chile'. MDV, MLP, SB, AP, LT and MT are partially supported by the PRIN-INAF 2011 with the project 'Transient Universe: from ESO Large to PESSTO'. This work was partly supported by the European Union FP7 programme through ERC grant number 320360.

This work is based (in part) on observations collected at the European Organization for Astronomical Research in the Southern hemisphere, Chile as part of PESSTO, ESO programme 188.D-3003, 191.D-0935. The research leading to these results has received funding from the European Research Council under the European Union's Seventh Framework Programme (FP7/2007-2013)/ERC Grant agreement no. [291222] (PI: S. J. Smartt) and STFC grants ST/I001123/1 and ST/L000709/1.

The early SN 2012ec data have been collected via the ESO-NTT Large Programme Supernova Variety and Nuclesosynthesis Yelds (184.D-1140), a European SN collaboration led by Stefano Benetti (http://sngroup.oapd.inaf.it/esolarge.html). This paper is partially based on observations collected at Copernico telescope (Asiago, Italy) of the INAF – Osservatorio Astronomico di Padova; at the Galileo 1.22m telescope operated by Department of Physics and Astronomy of the University of Padova at Asiago; at the 2.56m NOT operated by The Nordic Optical Telescope Scientific Association (NOTSA); at the 4.3m WHT operated by the Isaac Newton Group of Telescopes; on observations obtained through the CNTAC proposal CN2012B-73 and on observations made with the LT (programme OL12B) operated on the island of La Palma by Liverpool John Moores University in the Spanish Observatorio del Roque de los Muchachos of the Instituto de Astrofisica de Canarias with financial support from the UK Science and Technology Facilities Council.

REFERENCES

Arcavi I. et al., 2012, ApJ, 756, L30
Arnett W. D., Fu A., 1989, ApJ, 340, 396
Barbon R., Ciatti F., Rosino L., 1979, A&A, 72, 287
Baron E., Nugent P. E., Branch D., Hauschildt P. H., 2004, ApJ, 616, L91
Bayless A. J. et al., 2013, ApJ, 764, L13
Bersten M. C. et al., 2012, ApJ, 757, 31
Blinnikov S., Lundqvist P., Bartunov O., Nomoto K., Iwamoto K., 2000, ApJ, 532, 1132
Bose S. et al., 2013, MNRAS, 433, 1871
Botticella M. T. et al., 2010, ApJ, 717, L52
Bouchet P., Danziger I. J., Lucy L. B., 1991, AJ, 102, 1135
Cappellaro E., Evans R., Turatto M., 1999, A&A, 351, 459
Cardelli J. A., Clayton G. C., Mathis J. S., 1989, ApJ, 345, 245
Carpenter J. M., 2001, AJ, 121, 2851
Childress M., Scalzo R., Yuan F., Schimdt B., 2012, Cent. Bur. Electron. Telegrams, 3201, 2
Chugai N. N., Utrobin V. P., 2000, A&A, 354, 557
Coppola G. et al., 2011, MNRAS, 416, 1056
D'Andrea C. B. et al., 2010, ApJ, 708, 661
Dall'Ora M. et al., 2014, ApJ, 787, 139
Dessart L., Hillier D. J., 2005, A&A, 439, 671
Eastman R. G., Schmidt B. P., Kirshner R., 1996, ApJ, 466, 911
Elmhamdi A. et al., 2003a, MNRAS, 338, 939
Elmhamdi A., Chugai N., Danziger I. J., 2003b, A&A, 404, 1077
Faran T. et al., 2014, MNRAS, 442, 844
Filippenko A. V., 1997, ARA&A, 35, 309
Fraser M. et al., 2012, ApJ, 759, L13
Freedman W. L. et al., 2001, ApJ, 553, 47
Gilmozzi R. et al., 1987, Nature, 328, 318
Grassberg E. K., Imshennik V. S., Nadyozhin D. K., 1971, Ap&SS, 10, 28
Gustafsson B., Edvardsson B., Eriksson K., Jørgensen U. G., Nordlund Å., Plez B., 2008, A&A, 486, 951
Hamuy M., Pinto P., 2002, ApJ, 558, 615
Heger A., Fryer C. L., Woosley S. E., Langer N., Hartmann D. H., 2003, ApJ, 591, 288
Hook I. M., 2013, Phil. Trans. R. Soc. A, 371, 20282
Iben I., Renzini A., 1983, ARA&A, 21, 271
Inserra C. et al, 2011, MNRAS, 417, 261
Inserra C. et al, 2012, MNRAS, 422, 1122
Jerkstrand A., Fransson C., Maguire K., Smartt S., Ergon M., Spyromilio J., 2012, A&A, 546, A28
Jerkstrand A. et al., 2014a, preprint (arXiv:1410.8394)
Jerkstrand A., Smartt S. J., Fraser M., Fransson C., Sollerman J., Taddia F., Kotak R., 2014b, MNRAS, 439, 3694
Kasen D., Woosley S. E., 2009, ApJ, 703, 2205
King J. Y., Modjaz M., Shefler T., Halderson E., Li W. D., Treffers R. R., Filippenko A. V., 1998, Int. Astron. Union Circ., 6992, 1
Kirshner R. P., Kwan J., 1974, ApJ, 193, 27
Kirshner R. P., Sonneborn G., Crenshaw D. M., Nassiopoulos G. E., 1987, ApJ, 320, 602
Kleiser I. K. W. et al., 2011, MNRAS, 415, 372
Kochanek C. S., Khan R., Dai X., 2012, ApJ, 759, 20
Kowal C. T., 1968, AJ, 73, 1021
Landolt A. U., 1992, AJ, 104, 340
Li W., Cenko S. B., Filippenko A. V., 2009, Cent. Bur. Electro. Telegrams, 1656, 1
Li W. et al., 2011, MNRAS, 412, 1441
Litvinova I. Yu., Nadezhin D. K., 1983, Ap&SS, 89, 89
Litvinova I. Yu., Nadezhin D. K., 1985, Pis'ma Astron. Zh., 11, 351
Maguire K. et al., 2010, MNRAS, 404, 981
Massey P., Waterhouse E., DeGioia-Eastwood K., 2000, AJ, 119, 2214
Massey P., DeGioia-Eastwood K., Waterhouse E., 2001, AJ, 121, 1050
Maund J. R. et al., 2013, MNRAS, 413, L102
Mitchell R. C., Baron E., Branch D., Hauschildt P. H., Nugent P. E., Lundqvist P., Blinnikov S., Pun C. S. J., 2002, ApJ, 574, 293
Moiseev A. V., 2000, A&A, 363, 843
Monard L. A. G., 2012, Cent. Bur. Electron. Telegrams, 3201, 1
Nakano S., 2006, Cent. Bur. Electron. Telegrams, 470, 1
Nakano S., Aoki M., Kushida Y., Kushida R., Benetti S., Turatto M., van de Steene G., 1996, Int. Astron. Union Circ., 6442, 1
Nugent P. et al., 2006, ApJ, 645, 841
Olivares E. F. et al., 2010, ApJ, 715, 833
Pastorello A. et al., 2004, MNRAS, 347, 74
Pastorello A. et al., 2009a, MNRAS, 394, 2266
Pastorello A. et al., 2009b, A&A, 500, 1013
Pastorello A. et al., 2012, A&A, 537, A141
Perlmutter S. et al., 1999, ApJ, 517, 565
Poznanski D., 2013, MNRAS, 436, 3224
Poznanski D. et al., 2009, ApJ, 694, 1067
Poznanski D., Nugent P. E., Filippenko A. V., 2010, ApJ, 721, 956
Poznanski D., Prochaska J. X., Bloom J. S., 2012, MNRAS, 426, 1465
Pumo M. L., Zampieri L., 2011, ApJ, 741, 41

Pumo M. L., Zampieri L., Turatto M., 2010, Mem. Soc. Astron. Ital. Suppl., 14, 123
Quimby R. M., Wheeler J. G., Höflich P., Akerlof C. W., Brown P. J., Rykoff E. S., 2007, ApJ, 666, 1093
Riess A. G. et al., 1998, AJ, 116, 1009
Riess A. G. et al., 2011, ApJ, 730, 119
Rizzi L., Tully R. B., Makarov D., Makarova L., Dolphin A. E., Sakai S., Shaya E. J., 2007, ApJ, 661, 815
Roy R. et al., 2007, in Ray A., McCray R. A., eds, Proc. IAU Symp. 296, Supernova Environmental Impacts. Cambridge Univ. Press, Cambridge, p. 116
Rubin D. et al., 2013, ApJ, 763, 35
Schlafly E. F., Finkbeiner D. P., 2011, ApJ, 737, 103
Schlegel D. J., Finkbeiner D. P., Davis M., 1998, ApJ, 500, 525
Schmidt B. P., Kirshner R. P., Eastman R. G., 1994, ApJ, 432, 42
Schmidt B. P., Suntzeff N. B., Phillips M. M., 1998, ApJ, 507, 46
Skrutskie M. F. et al., 2006, AJ, 131, 1163
Smartt S. J., 2009, ARA&A, 47, 63
Smartt S. J., Eldridge J. J., Crockett R. M., 2009, MNRAS, 395, 1409
Smartt S. J. et al., 2014, preprint (arXiv:1411.0299)
Smith J. A., Tucker D. L., Kent S., 2002, AJ, 123, 2121
Spiro S, Pastorello A., Pumo M. L., 2014, MNRAS, 439, 2873
Stetson P. B., 1987, PASP, 99, 191
Suntzeff N. B., Hamuy M., Martin G., Gomez A., Gonzalez R., 1988, AJ, 96, 1864
Tammann G. A., Reindl B., 2013, A&A, 549, A136
Tomasella L. et al., 2013, MNRAS, 434, 1636
Tully R., Rizzi L., Shaya E. J., Courtois H. M., Makarov D. I., Jacobs B. A., 2009, AJ, 138, 323
Turatto M., Benetti S., Cappellaro E., 2003, in Hillebrandt W., Leibundgut B., eds, From Twilight to Highlight: The Physics of Supernovae. Springer, Berlin, p. 200
Utrobin V. P., 1993, A&A, 281, L89
Utrobin V. P., 2007, A&A, 461, 233
Utrobin V. P., Chugai N. N., 2008, A&A, 491, 507
Utrobin V. P., Chugai N. N., 2009, A&A, 506, 829
Utrobin V. P., Chugai N. N., Pastorello A., 2007, A&A, 475, 973
Valenti S. et al., 2011, MNRAS, 416, 3138
Van Dyk S. D. et al., 2012, ApJ, 756, 131
Walmswell J. J., Eldridge J. J., 2012, MNRAS, 419, 2054
Weaver T. A., Woosley S. E., 1980, in Hugh C., Roland E., Wolfe M., Gillepsie G. H., eds, AIP Conf. Proc. Vol. 63, Supernovae Spectra. Am. Inst. Phys., New York, p. 15
Woosley S. E., Heger A., Weaver T. A., 2002, Rev. Mod. Phys., 74, 1015
Yaron O., Gal-Yam A., 2012, PASP, 124, 668
Zampieri L., 2005, in Turatto M., Benetti S., Zampieri L., Shea W., eds, ASP Conf. Ser. Vol. 342, 1604-2004: Supernovae as Cosmological Lighthouses. Astron. Soc. Pac., San Francisco, p. 358
Zampieri L., 2007, in Antonelli L. A. et al., eds, AIP Conf. Ser. Vol. 924, The Multicolored Landscape of Compact Objects and their Explosive Origins. Am. Inst. Phys., New York, p. 358
Zampieri L., Shapiro S. L., Colpi M., 1998, ApJ, 502, L149
Zampieri L., Pastorello A., Turatto M., Cappellaro E., Benetti S., Altavilla G., Mazzali P., Hamuy M., 2003, MNRAS, 338, 711

[1]*Dip. di Fisica and ICRA, Sapienza Universitá di Roma, Piazzale Aldo Moro 5, I-00185 Rome, Italy*
[2]*INAF – Osservatorio Astronomico di Capodimonte, Salita Moiariello 16, I-80131 Napoli, Italy*
[3]*ICRANet – Pescara, Piazza della Repubblica 10, I-65122 Pescara, Italy*
[4]*INAF – Osservatorio Astronomico di Padova, Vicolo dell'Osservatorio 5, I-35122 Padova, Italy*
[5]*Department of Physics and Astronomy, University of Sheffield, Sheffield S3 7RH, UK*
[6]*Astrophysics Research Centre, School of Mathematics and Physics, Queen's University Belfast, Belfast BT7 1NN, UK*
[7]*Institute of Astronomy, University of Cambridge, Madingley Road, Cambridge CB3 0HA, UK*
[8]*Department of Particle Physics and Astrophysics, The Wiezmann Institute of Science, Rehovot 76100, Israel*
[9]*Millennium Institute of Astrophysics, Vicuña Mackenna 4860, 7820436 Macul, Santiago, Chile*
[10]*Departamento de Astronomía, Universidad de Chile, Camino el Observatorio 1515, Casilla 36-D, Santiago, Chile*
[11]*INAF – Osservatorio Astronomico di Trieste, Via Tiepolo Giambattista 11, I-34131 Trieste, Italy*
[12]*Department of Physics and Astronomy, University of North Carolina at Chapel Hill, Chapel Hill, NC 27599-3255, USA*
[13]*Departamento de Ciencias Fisicas, Universidad Andres Bello, Avda Republica 252, 32349 Santiago, Chile*
[14]*Universitäts-Sternwarte München, Scheinerstr. 1, D-81679 München, Germany*
[15]*Research School of Astronomy and Astrophysics, Australian National University, Cotter Road, Weston Creek, ACT 2611, Australia*
[16]*The Oskar Klein Centre, Department of Astronomy, Stockholm University, Albanova, SE-10691 Stockholm, Sweden*
[17]*School of Physics and Astronomy, University of Southampton, Southampton SO17 1BJ, UK*
[18]*Las Cumbres Observatory Global Telescope Network, 6740 Cortona Dr., Suite 102, Goleta, CA 93117, USA*

This paper has been typeset from a TEX/LATEX file prepared by the author.